Dalton Transactions

ROYAL SOCIETY OF CHEMISTRY

PAPER

View Article Online
View Journal | View Issue

Cite this: *Dalton Trans.*, 2020, **49**, 6668

Bulky 1,1′-bisphosphanoferrocenes and their coordination behaviour towards Cu(I)†‡

Subhayan Dey,[a] Daniel Buzsáki,[b] Clemens Bruhn,[a] Zsolt Kelemen *[b] and Rudolf Pietschnig *[a]

Received 12th March 2020,
Accepted 7th April 2020

DOI: 10.1039/d0dt00941e

rsc.li/dalton

Two bulky mesityl substituted dppf-analogues $Fe(C_5H_4PMes_2)_2$ (Mes = 2,4,6-$Me_3C_6H_2$, **1**) and $Fe(C_5H_4PMes_2)(C_5H_4PPh_2)$ (Mes = 2,4,6-$Me_3C_6H_2$, Ph = C_6H_5, **3**) have been prepared and their properties as donor ligands have been explored using heteronuclear NMR spectroscopy and in particular *via* $^1J_{P-Se}$ coupling, cyclic voltammetry and DFT calculations. Based on the results obtained, a series of mono- and dinuclear Cu(I) complexes have been prepared with these new diphosphane ligands using Br^-, I^-, and BF_4^- as counter anions. For the very bulky ligand **1** rare and unprecedented double bridging complexation modes have been observed containing two non-planar Cu_2Br_2 units, while for the other dinuclear complexes planar Cu_2Br_2 units have been found. The Cu(I) complexes of **1** and **3** were then used as catalysts for CO_2-fixation reaction with terminal alkynes, and complexes with ligand **3** were found to be more efficient than those with **1**. DFT calculations performed on compounds **1**, **3** and their Cu(I) complexes were able to verify the trend of these catalytic reactions.

Introduction

Being an extremely useful and unique building block, ferrocene has remained a center of attraction for several decades. Apart from the fact that it is important for synthesizing organometallic polymers,[1–5] redox-tunable substances,[4,6–8] drugs,[9,10] and other functional materials,[11–14] ferrocene has played a vital role in homogeneous catalysis.[15,16] Diphosphane ligand systems have emerged from their monophosphane counterparts, and ferrocene has provided them with an unprecedented backbone,[17–19] which helped to stabilize a variety of metal centers by forming flexible geometries.[15,20] This special arrangement has further been appreciated, when it emerged that the bite angles (β_n, **A**, Fig. 1) of such ligands, which have an apparent positive effect on the efficiency of catalysts,[21,22] can be manipulated by changing the substituents on phosphorus.[23] Systematic investigations further revealed that the alteration of substituents on phosphorus can be achieved by simple and modular synthetic approaches.[23,24] The aforementioned qualities made ferrocene-based diphosphane ligands remarkably successful for homogeneous catalysis.[15,16] The quest for new ligands, with ideal steric demand and optimum donating ability, is still ongoing.[25–30]

Although many different 1,1′-symmetrically and unsymmetrically substituted bisphosphanoferrocenes have been reported in the past (**B** and **C**, Fig. 1),[19,23,25,31–40] the catalytic discussions have been dominated by 1,1′-bis(diphenylphosphano)ferrocene (dppf, **D**, Fig. 1) for many decades.[15,16,24] However, in 2007, it was reported that 1,1′-bis(di-*tert*-butylpho-

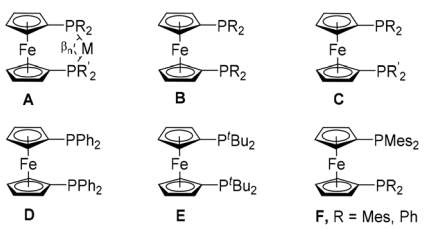

Fig. 1 Bite angle (β_n, **A**),[21,22] previously (**B–E**),[23] and herein reported (**F**) achiral 1,1′-bisphosphanoferrocene ligands. Known symmetrically substituted dppf analogues (**B**): R = Me,[17] Et,[34] ^{i}Pr,[31,45] Cy,[19] ^{t}Bu,[32] *o*-tolyl,[33,46] *o*-MeO–C_6H_4,[34] *p*-MeO–C_6H_4,[47] *p*-PhO–C_6H_4,[46] *p*-CF_3–C_6H_4,[48] 3,5-CF_3–C_6H_3,[33] 2-furyl,[33] 5-Me-2-furyl,[37] *o*-^{i}Pr-C_6H_4,[34] 1-Nap,[46] 2-Nap,[46] C_6F_5.[34] Known 1,1′-unsymmetrically substituted dppf analogues (**C**): R = Ph, R′ = ^{t}Bu;[35,36] R = Ph, R′ = ^{i}Pr;[25] R = Ph, R′ = Cy;[25] R = Ph, R′ = *p*-MeO–C_6H_4;[38] R = Ph, R′ = 5-Me-2-furyl;[37] R = Ph, R′ = Cl;[39] R = Ph, R′ = OPh;[40] R = Ph, R′ = OMen;[39] R = Ph, R′ = *p*-Me–Ph;[38] R = *p*-Me–Ph, R′ = *p*-CF_3–Ph.[38]

[a]*Institut für Chemie und CINSaT, University of Kassel, Heinrich Plett-Straße 40, 34132 Kassel, Germany. E-mail: pietschnig@uni-kassel.de*
[b]*Department of Inorganic and Analytical Chemistry, Budapest University of Technology and Economics, and MTA-BME Computation Driven Chemistry Research Group, Szent Gellért tér 4, 1111 Budapest, Hungary*

† Dedicated to Professor Manfred Scheer on the occasion of his 65th birthday.

‡ Electronic supplementary information (ESI) available: NMR spectra, crystal structures of **4** and **6**, crystal refinement data, CV and details of DFT calculations. CCDC 1980151–1980158 contains the supplementary crystallographic data for compounds **3–6**, **10**, and **12–14**. For ESI and crystallographic data in CIF or other electronic format see DOI: 10.1039/D0DT00941E

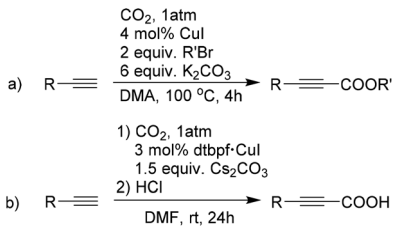

Scheme 1 Cu-catalyzed carboxylation of terminal alkynes.[50]

sphano)ferrocene (dtbpf, **E**, Fig. 1) is superior to dppf for the Pd-catalyzed α-arylation of ketones and certain Pd-catalyzed Suzuki coupling reactions.[41,42] Moreover, in the recent past, several reports have theoretically proved the fact that with the increase of the steric bulk on phosphorus, the donating ability and β_n increase, and as a result the catalytic activity increases.[43,44] In this context, two obvious questions arise: (1) what is the maximum attainable sterics before the complexation of 1,1′-bisphosphanoferrocene compromises? (2) How much steric bulk can be used without affecting the catalytic activity of the resulting complexes? Since the steric situation will differ from one metal to the other, we have explored a catalytic process and addressed the above questions using two novel sterically congested 1,1′-diphosphanoferrocene ligands, namely 1,1′-bis(dimesitylphosphano)ferrocene and 1-(dimesitylphosphano)-1′-(diphenylphosphano)ferrocene. The complete syntheses of these ligands and their electrochemical properties and donating abilities will be reported herein, and the first insight into their potential for catalysis will be provided.

Owing to current interest in using CO_2 as sustainable feedstock in catalytic transformations, we set out to investigate the catalytic formation of propiolic acid derivatives from CO_2 and terminal alkynes. The first report of such catalytic CO_2-fixation reactions was published by the Inoue group in 1994, where CuI was used as a catalyst (Scheme 1a).[49] Although the insertion of CO_2 into alkynylcopper was successful, high temperature and a large excess of base were needed for the execution of this reaction.[49,50] Recently, Rath *et al.* have reported similar carboxylation reactions with Cu-complexes of dtbpf, where ambient temperatures have been used for high yielding transformations (Scheme 1b).[51] Considering the fact that copper is an affordable late transition metal and potentially active for the reaction of our interest,[50,52,53] we first decided to synthesize the CuX (X = Br, I, $(MeCN)_nBF_4$) complexes of our ligands. The structural properties of these complexes and their catalytic behaviour have been further studied in this report. Finally, to obtain an insight into the energetic scenario of complexation and the related catalysis, we have used density functional theory (DFT), which further helped us to verify the experimentally obtained results.

Results and discussion

Syntheses and complexation

A few 1,1′-substituted ferrocenyl compounds with two dimesitylphosphanyl groups have been previously synthesized by

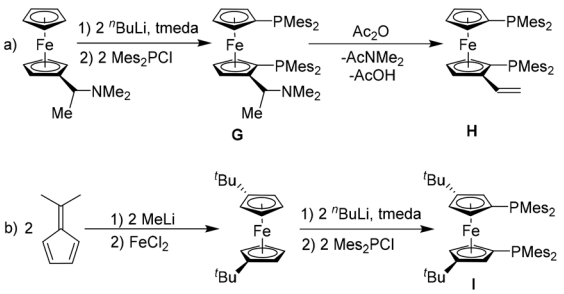

Scheme 2 Syntheses of substituted 1,1′-bis(dimesitylphosphano)ferrocenes *via* routes (a) and (b).[54,55]

reacting modified dilithioferrocene with Mes_2PCl as reagents (**G**, **H** and **I**, Scheme 2).[54,55] However, their properties as bidentate ligands in metal complexation and homogeneous catalysis have not been explored in detail, except for a few instances of silver-mediated nucleophilic fluorination.[55]

The synthesis of our mesityl-substituted bisphosphano ligand **1** was carried out by two complementary pathways. The first pathway involves PCl_2-substituted ferrocene **2**, which was synthesized by a known method[56,57] and subsequently reacted with four equivalents of MesLi·LiBr·OEt_2 (Scheme 3a). On the other hand, the second pathway (Scheme 3b) uses tmeda-stabilized dilithioferrocene, which was reacted with two equivalents of Mes_2PX (X = Cl and Br). Although both the pathways can produce **1** in an acceptable purity, the first pathway (Scheme 3a) gives a slightly higher yield than the second (Scheme 3b).

The unsymmetrically substituted bisphosphano ligand **3** was synthesized by following a simple and modular approach (Scheme 3c). At first, compound **4** was synthesized by selective monolithiation of 1,1′-dibromoferrocene[58] and subsequent *in situ* reaction with Mes_2PX. When compound **4** was further monolithiated and *in situ* reacted with Ph_2PCl, compound **3** was obtained in an overall yield of 33%, starting from 1,1′-dibromoferrocene.

In order to explore the donating abilities of our ligands, the selenophosphorane derivatives of **1** and **3** were synthesized by

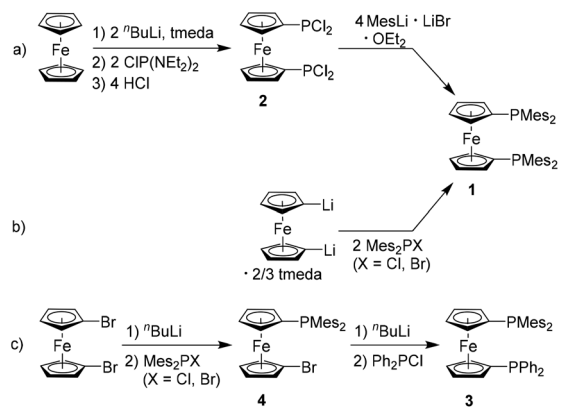

Scheme 3 Syntheses of mesityl-substituted bisphosphano ligands **1** and **3**.

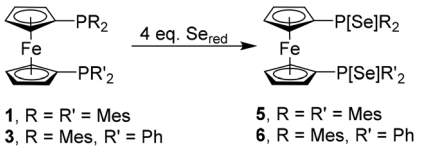

Scheme 4 Syntheses of diselenide derivatives of **5** and **6**.

adapting a reported procedure (Scheme 4), and their $^{1}J_{P-Se}$ values were compared with selenides of other phosphane ligands.[59,60] Since compounds **5** and **6** are not soluble in common NMR solvents like $CDCl_3$ and C_6D_6, our comparison became restricted to data available for toluene solutions. To this end we recorded the ^{31}P and ^{77}Se NMR spectra of $Ph_3P[Se]$ and dppf$[Se]_2$ in toluene as the benchmark for this comparison as well, since the underlying phosphanes Ph_3P and dppf are extremely popular and useful ligands in many synthetic applications.[15,16,61–77] The $^{1}J_{P-Se}$ for compound **5** (723 Hz) is significantly lower than the corresponding values for $Ph_3P[Se]$ (732 Hz in $CDCl_3$;[78] 758 Hz in toluene-d8, see Fig. S61 in ESI file‡) and dppf$[Se]_2$ (737 Hz in $CDCl_3$;[59,79] 761 Hz in toluene-d8, see Fig. S59 in ESI file‡), which indicates that the lone pairs of phosphorus centres in **1** have a lower s character, and therefore, a higher donating ability than Ph_3P and dppf. A similar trend could also be noticed for the ^{77}Se NMR chemical shifts, where the resonance of compound **5** at −82 ppm is deshielded by *ca.* δ 200 ppm and 220 ppm, compared to $Ph_3P[Se]$ and dppf$[Se]_2$, respectively (see Fig. S21, S62 and S60 in the ESI file‡), which are in fact closer to values observed for the selenides of push pull substituted phosphanes.[60]

In line with the lower symmetry in compound **6**, two different values of $^{1}J_{P-Se}$ have been observed: 723 Hz for $Mes_2P[Se]$ and 763 Hz for $Ph_2P[Se]$, which are coherent with the corresponding values for **5** and dppf$[Se]_2$, respectively. The ^{77}Se NMR spectra of compound **6** show a set of two doublets, for the Se atoms at the two different phosphorus centres at −78 ppm ($PSeMes_2$) and −299 ppm ($PSePh_2$), which are consistent with the values observed for **5** and dppf$[Se]_2$ (see Fig. S21, S25 and S60 in ESI file‡). It should be noted that although the $^{1}J_{P-Se}$ values for dtbpf$[Se]_2$,[80] dippf$[Se]_2$ (dippf = 1,1′-bis(di-iso-propylphosphano)ferrocene),[81] dchpf$[Se]_2$ (dchpf = 1,1′-bis(dicyclohexylphosphano)ferrocene),[82] dchpdppf$[Se]_2$ [dchpdppf = 1-(dicyclohexylphosphano)-1′-(diphenylphosphano)ferrocene],[25] dippdppf$[Se]_2$ [dippdppf = 1-(diisopropylphosphano)-1′-(diphenylphosphano) ferrocene],[25] and dppdtbpf$[Se]_2$ [dppdtbpf = 1-(diphenylphosphano)-1′-(di-*tert*-butylphosphano)ferrocene][25] were reported in the literature, they were measured in $CDCl_3$ and therefore could not be considered for this comparison.

Suitable single crystals for X-ray analyses were obtained for compounds **3–6**. Fig. 2 and 3 show the molecular structures of **3** and **5** respectively, and their refinement data are listed in Table S1 (ESI file‡). The molecular structure of **3** in the solid state shows a sum of angles of 311.98(15)° at the phosphorus atom of the $PMes_2$ unit which is larger than the respective

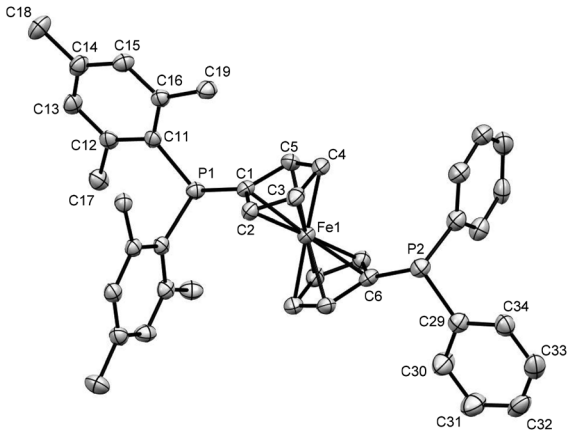

Fig. 2 Ortep plots of the molecular structures of **3** in the solid state with ellipsoids drawn at the 50% probability level. Labels for some selected C atoms, solvent molecules and H atoms are omitted for clarity. Selected bond lengths [Å] and angles [°]: C(1)–C(2) 1.428(5), C(1)–P(1) 1.816(3), C(11)–P(1) 1.850(3), C(11)–C(16) 1.418(5), C(15)–C(16) 1.391(5), C(14)–C(15) 1.382(5), C(16)–C(19) 1.504(5), C(6)–P(2) 1.823(3), C(29)–P(2) 1.835(4), C(29)–C(34) 1.394(5), C(33)–C(34) 1.384(5), C(32)–C(33) 1.372(6), C(5)–C(1)–P(1) 122.7(3), C(1)–P(1)–C(11) 108.70(15), P(1)–C(11)–C(16) 127.6(2), C(6)–P(2)–C(29) 101.70(15).

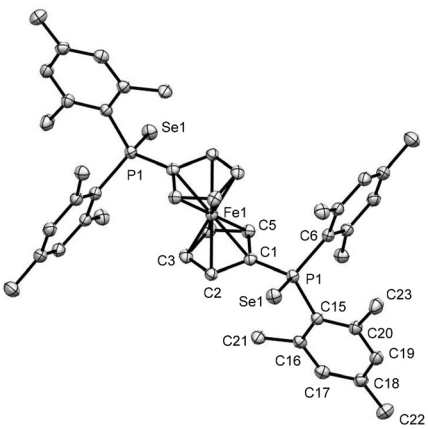

Fig. 3 Ortep plots of the molecular structures of **5** in the solid state with ellipsoids drawn at the 50% probability level. Labels for some selected C atoms, solvent molecules and H atoms are omitted for clarity. Selected bond lengths [Å] and angles [°]: P(1)–C(1) 1.798(2), P(1)–Se(1) 2.1216(6), P(1)–C(6) 1.847(2), C(15)–C(20) 1.411(3), C(20)–C(23) 1.507(3), C(1)–C(5) 1.440(3), C(1)–Fe(1) 2.051(2), C(1)–P(1)–Se(1) 109.11(7), C(1)–P(1)–C(6) 102.94(10), C(1)–P(1)–C(15) 112.25(10), C(1)–P(1)–C(15) 112.25(10), C(6)–P(1)–Se(1) 122.09(7), C(15)–P(1)–Se(1) 106.20(7).

value for the PPh_2 unit in the same molecule (303.37(16)°), indicating increased steric interaction in the former.

Similar trends are found for **5** and **6** which are the selenophosphorane derivatives of **1** and **3**. The sum of the C–P–C angles in **5** carrying two $PSeMes_2$ units is 319.5(1)° which is almost identical to the corresponding value of the $PSeMes_2$ unit in mixed substituted **6** (321.8(3)°), while the $PSePh_2$ unit shows only 315.2(2)°. Consistent with these findings the P–Se bond lengths are slightly longer in the sterically more demand-

ing $PSeMes_2$ units (**5**: 2.1216(6) Å, **6**: 2.1246(14) Å) than in the $PSePh_2$ unit (**6**: 2.0971(13) Å). These structural features indicate a more pronounced dative P–Se interaction for PPh_2 than for the $PMes_2$ unit in agreement with the NMR data outlined above, where the sterically less hindered phosphane unit entails larger $^1J_{P-Se}$ coupling values and stronger shielding of the ^{77}Se resonance in the corresponding selenophosphorane. The solid-state structures of **4** and **6** are included in the ESI file (Fig. S65 and S66‡).

To explore the overall electronic effect of replacing phenyl with mesityl units in this molecular scaffold, the redox properties of the metallocene unit have been investigated using cyclic voltammetry (CV). The results, obtained by CV investigation, were further clarified by DFT calculations using the ω-B97XD/6-311+G** level of theory (more details in the ESI file‡) as the oxidation of P(III) substituted ferrocenes may involve iron or phosphorus centred redox events.[83–89] The oxidation reactions of compounds **1** and **3** occur at 0.13 V and 0.16 V (see Fig. S69 and S70 in ESI file‡), respectively, which are slightly shifted to lower potentials in comparison to that of dppf (E° = 0.18 V). By investigating the Kohn–Sham molecular orbitals of **1**, **3** and the parent dppf, it could be established that the lone pairs of the phosphorus atoms make a significant contribution to the HOMO (Fig. 4, Fig. S71 and S72 in ESI file‡). In agreement with the increased bond angles around phosphorus in the case of $PMes_2$ units, the energy of this lone pair increases, thus contributing more to the HOMOs as well. This was in full agreement with the slightly shifted oxidation potentials of **1** and **3**. The calculated spin density distribution of the corresponding cations of **1** and **3** is extensively localised at the iron center (Fig. S73 in ESI‡), and thus the iron centred redox process is reversible for compound **3** (Fig. S70 in ESI file‡) and quasi-reversible for compound **1** (Fig. S69 in ESI file‡). Moreover, for both complexes, several follow up oxidation processes can be found at higher anodic potentials, which are likely to involve PR_2 moieties, in agreement with the significant contribution of the phosphorus lone pairs to the HOMO of the corresponding dicationic species. These follow up oxidations are irreversible and show small anodic shifts during reduction. To further characterize our ligands NBO calculations were performed, which revealed that upon changing the two phenyls to two mesityl groups, the p-character of the phosphorus lone pairs increased from 53% for dppf to 55–56% for **1** and **3** (Table S4 in ESI file‡). Recently it has been shown that the electronic effects of phosphorus containing bidentate ligands can be described by calculating the CO-stretching frequencies of the corresponding L_2PdCO complexes (analogously to the experimental Tolman parameter).[43] This method (more details in the ESI file‡) has further been used to show that the electron donating ability increases from dppf to **1** and **3** in the order of dppf < **3** < **1** (Table S4 in ESI file‡).

The previous findings classify **1** and **3** as electron rich ligand systems with increased steric congestion along with the increased p-character of the phosphorus lone pair for the $PMes_2$ unit. To explore their ligand properties towards d-block

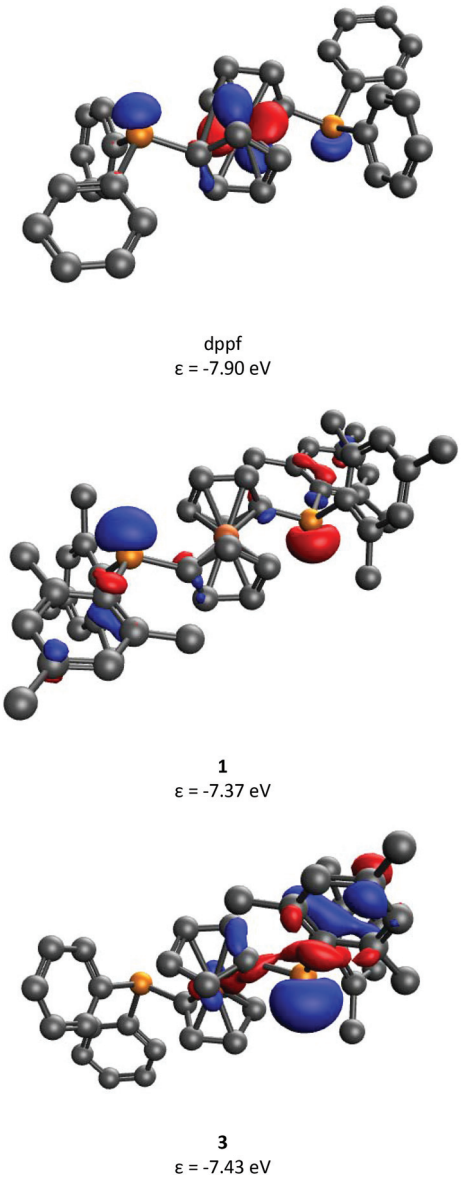

Fig. 4 The Kohn–Sham HOMOs of dppf, **1** and **3** (structures were optimized at the ω-B97XD/6-311+G** level of theory). Hydrogen atoms are omitted for clarity.

metals and possible effects on catalytic systems, Cu(I) complexes have been chosen, owing to their proclivity to adopt small coordination numbers for which steric effects should be less decisive. Using a common synthetic methodology, CuX-complexes **7**–**12** (X = Br, I, $(MeCN)_nBF_4$, Scheme 5) were synthesized from ligands **1** and **3**. Among them, the solid state structures could only be obtained for complexes **10** and **12**, which are depicted in Fig. 5 and 6, respectively. Although no suitable single crystals for X-ray analysis could be isolated for complexes **7**–**9**, their formation was indicated by the upfield shifts of ^{31}P signals (from δ −33.5 for **1** to δ −26.8 for **7**, δ −25.0 for **8** and δ −27.8 for **9**; see Fig. S8, S28, S31 and S34 in ESI file‡). Moreover, the broad lines in their ^{1}H and ^{31}P NMR spectra (see Fig. S26–S34 in ESI file‡) suggest a fast exchange

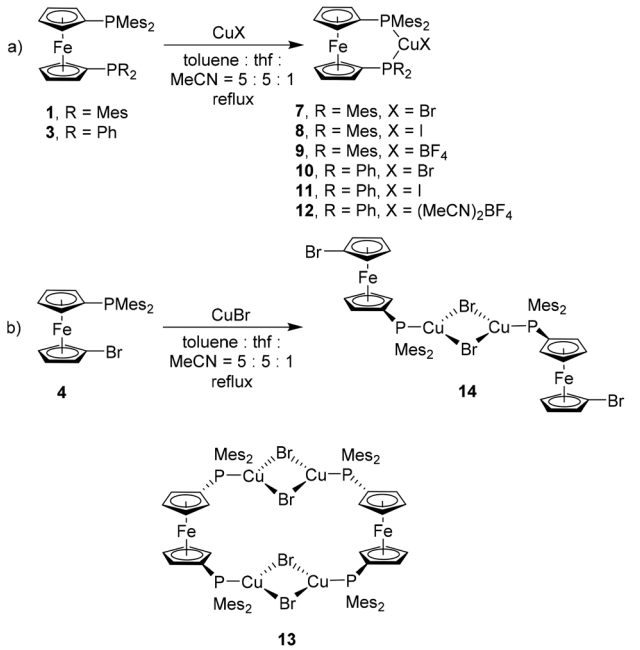

Scheme 5 CuX-complexes (X = Br, I, $(MeCN)_nBF_4$) of **1**, **3** (eqn a) and **4** (eqn b).

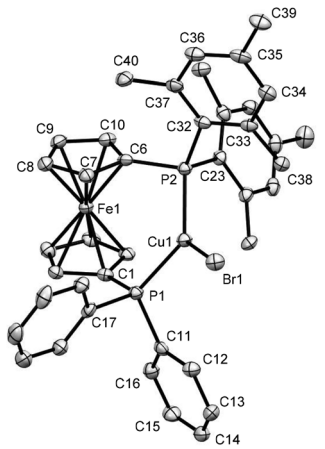

Fig. 5 Ortep plots of the molecular structures of **10** in the solid state with ellipsoids drawn at the 50% probability level. Labels for some selected C atoms, solvent molecules and H atoms are omitted for clarity. The refinement data for this structure can be found in Table S2 (ESI file‡). Selected bond lengths [Å] and angles [°]: C(1)–P(1) 1.816(5), C(11)–P(1) 1.827(5), Cu(1)–P(1) 2.2540(15), Cu(1)–Br(1) 2.3428(9), Cu(1)–P(2) 2.2651(15), C(23)–P(2) 1.843(5), C(6)–P(2) 1.820(6), C(6)–P(2)–C(23) 103.7(2), C(23)–P(2)–C(32) 104.0(2), C(23)–P(2)–Cu(1) 120.25(17), C(32)–P(2)–Cu(1) 112.91(17), C(6)–P(2)–Cu(1) 104.52(17), C(6)–P(2)–C(32) 111.0(2), C(1)–P(1)–Cu(1) 115.88(17), C(1)–P(1)–C(11) 103.4(2), C(1)–P(1)–C(17) 102.4(2), C(11)–P(1)–Cu(1) 116.86(17), C(11)–P(1)–C(17) 102.4(2), P(1)–Cu(1)–Br(1) 113.81(5), P(2)–Cu(1)–Br(1) 128.24(5), P(1)–Cu(1)–P(2) 116.53(6).

of Cu^+ ions in the solution. On the other hand, the formation of complex **11** could be confirmed by the shifts and multiplicities of its ^{31}P signals [from δ −35.1 (s), −17.2 (s) for **3** to δ −30.1 (brm), −20.2 (d) for **11**, see Fig. S17 and S45 in ESI file‡],

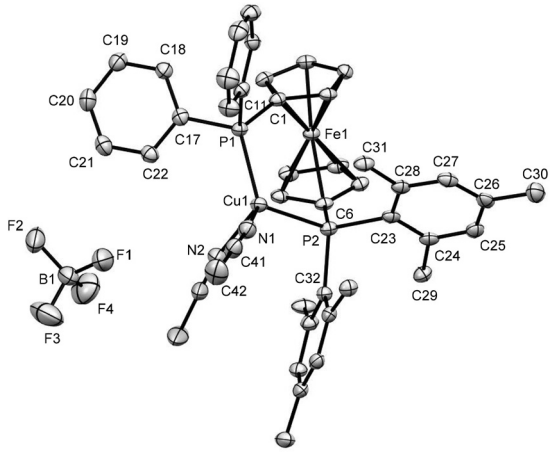

Fig. 6 Ortep plots of the molecular structures of **12** in the solid state with ellipsoids drawn at the 50% probability level. One of the two coordinated acetonitrile molecules is disordered in the CCH_3 part, for which only one position is shown without labels. Other solvent molecules and H atoms are omitted for clarity. The refinement data for this structure can be found in Table S2 (ESI file‡). Selected bond lengths [Å] and angles [°]: C(1)–P(1) 1.803(3), C(11)–P(1) 1.829(3), Cu(1)–P(1) 2.2437(8), Cu(1)–P(2) 2.3302(8), C(6)–P(2) 1.818(3), C(23)–P(2) 1.853(3), Cu(1)–N(1) 2.018(3), C(6)–P(2)–Cu(1) 103.33(10), C(6)–P(2)–C(23) 103.77(13), C(32)–P(2)–C(23) 104.36(13), C(6)–P(2)–C(32) 112.34(13), C(32)–P(2)–Cu(1) 103.22(9), C(1)–P(1)–Cu(1) 113.69(10), C(1)–P(1)–C(11) 102.41(13), C(1)–P(1)–C(17) 103.13(14), C(17)–P(1)–Cu(1) 117.22(10), P(1)–Cu(1)–P(2) 114.65(3), N(1)–Cu(1)–N(2) 91.98(12), P(1)–Cu(1)–N(1) 115.34(8), P(1)–Cu(1)–N(2) 118.70(9), F(1)–B(1)–F(2) 108.9(3), F(1)–B(1)–F(4) 112.5(4), F(2)–B(1)–F(3) 110.3(4).

which suggest a coupling between the two non-equivalent phosphorus atoms. It is needless to say that the evidence of a similar P–P coupling could also be noticed for complexes **10** and **12** (see Fig. S42 and S48 in ESI file‡).

The X-ray crystal structures of **10** and **12** revealed that the copper atoms are bonded to two phosphorus units with bite angles 116.53(6)° and 114.65(3)°, respectively (see Fig. 5 and 6). As the mesityl group is bulkier than phenyl, the Cu–P bond in the $P(Mes)_2$ unit [2.2651(15) Å for **10** and 2.3302(8) Å for **12**] is slightly longer (1 pm for **10** and 9 pm for **12**) than a similar bond in the PPh_2 unit [2.2540(15) Å for **10** and 2.2437(8) Å for **12**], which introduces a lower symmetry in complexes **10–12** for which a certain hemilability may be anticipated. To the best of our knowledge, there are only two complexes reported in the literature in which the ligands show a larger bite angle than **10** and both of them are based on dtbpf.[20,51,90] For comparison, a few related complexes, ordered by increasing bite angles (in parentheses), are listed in the following: $[Cu_2(\mu\text{-}SCN)_2(\kappa^2\text{-}P,P\text{-}dppf)_2]$ (112.13(4)°),[20,91] $[Cu_2(\mu_2\text{-}SCN)_2(\kappa^2\text{-}P,P\text{-}dppdtbpf)_2]$ (112.82(3)°),[90] $[Cu_2(\mu\text{-}CN)_2(\kappa^2\text{-}P,P\text{-}dppf)_2]$ (115.85(3)°),[92] $[Cu(\kappa^2\text{-}P,P\text{-}dppdtbpf)(CH_3CN)_2]PF_6$ (116.36(8)°),[90] $[Cu_2(\mu\text{-}NO_3\text{-}O)_2(\kappa^2\text{-}P,P\text{-}dppf)_2]$ (117.8(1)°),[93] and [CuI(dtbpf)] (120.070(19))°.[51]

Upon recrystallization of complex **7**, crystals of complex **13** formed (see Scheme 5), along with micro-crystalline and powdery by-products. The X-ray crystal-structure of complex **13**

shows a combination of 'double-bridge' and 'quasi-closed bridge' modes of coordination,[15] where two molecules of ligand **1** are connected *via* two diamond shaped (Cu_2Br_2) units (Fig. 7). In order to avoid the formation of complex **13**, several steps have been taken, such as changing the condition of crystallization and reaction of **1** with sub-stoichiometric amounts of CuBr (**28** : CuBr = 1 : 0.8, 1 : 0.7 and 1 : 0.5). However, all these experiments resulted in complex **13** as the only crystalline product and **13** can be prepared in a straightforward manner using an appropriate stoichiometry of metal to ligand.

The complexation *via* the formation of Cu_2X_2 (X = Cl, Br, I) bridges is common for dppf[51,92–96] and some sterically encumbered dppf analogues.[90,97–99] However, apart from this rare bonding motif, the classical chelating coordination mode of a single metal centre is also known for them.[25,90,100] For the [Mes_2P]-substituted ferrocene ligands, the formation of Cu_2X_2 bridges seems to be favoured as non-chelating ligand **4** similarly results in this motif for complex **14**, which was synthesized by reacting **4** with one equivalent of CuBr. X-ray crystallographic analysis revealed that this complex shows a similar bonding motif to **13**, where two molecules of **4** are bridged by one planar Cu_2Br_2 unit (Fig. 8). The distances between the Cu atoms in the Cu_2Br_2 moieties of complexes **13** and **14** are *ca.* 2.93 and 3.07 Å, respectively. These values are significantly lower, compared to the similar Cu–Cu distances of other halogen-bridged complexes reported in the literature.[92,94–96]

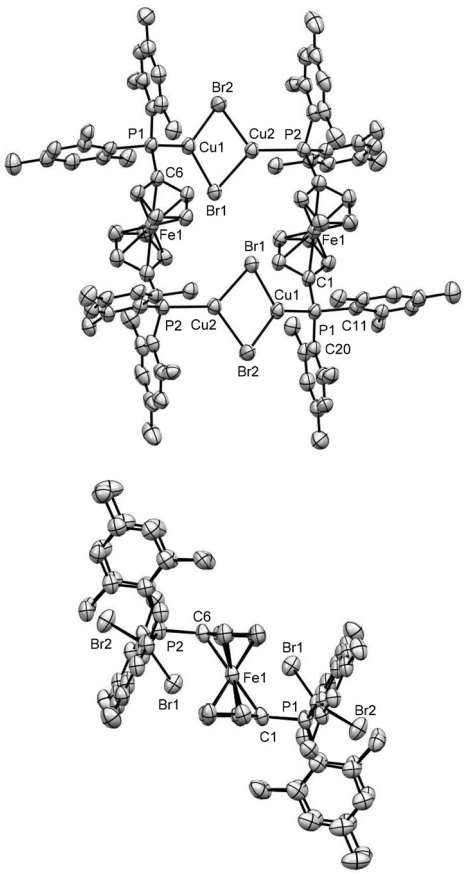

Fig. 7 Ortep plot of the molecular structure of **13** in the solid state with ellipsoids drawn at the 50% probability level. Labels for some selected C atoms, solvent molecules and H atoms are omitted for clarity. The figure at the top shows the [Cu_2Br_2] bridges, and the figure at the bottom shows the side view of the molecule. The plane of symmetry, passing through the four Br atoms, made this molecule achiral. The refinement data for this structure can be found in Table S2, ESI file.‡ Selected bond lengths [Å] and angles [°]: C(1)–P(1) 1.804(6), C(11)–P(1) 1.831(6), Cu(1)–P(1) 2.2095(16), Cu(2)–P(2) 2.2059(15), Cu(1)–Br(1) 2.3949(10), Cu(1)–Cu(2) 2.9295(11), C(1)–P(1)–C(11) 102.7(3), C(1)–P(1)–C(20) 110.4(3), C(1)–P(1)–Cu(1) 110.21(19), Cu(1)–P(1)–C(11) 121.37(19), Cu(1)–P(1)–C(20) 103.6(2), C(20)–P(1)–C(11) 108.5(3), P(1)–Cu(1)–Br(1) 131.98(5), P(1)–Cu(1)–Br(2) 124.84(5), Br(1)–Cu(1)–Br(2) 102.34(4), Cu(1)–Br(1)–Cu(2) 74.46(3), Cu(2)–Cu(1)–Br(1) 53.57(3).

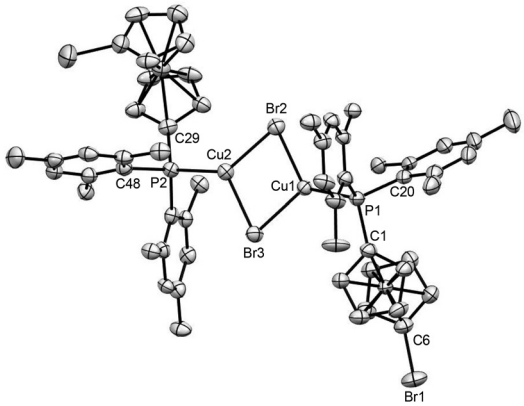

Fig. 8 Ortep plot of the molecular structure of **14** in the solid state with ellipsoids drawn at the 50% probability level. Labels for some selected C atoms, solvent molecules and H atoms are omitted for clarity. The refinement data for this structure are listed in Table S2 (ESI file‡), and the side view of this molecule is shown in Fig. S67 (ESI file‡). The refinement data for this structure can be found in Table S2, ESI file.‡ Selected bond lengths [Å] and angles [°]: C(1)–P(1) 1.815(6), C(20)–P(1) 1.842(6), Cu(1)–P(1) 2.2044(15), Cu(1)–Br(2) 2.4592(9), Br(1)–C(6) 1.886(6), C(1)–P(1)–Cu(1) 111.33(18), C(1)–P(1)–C(20) 102.1(3), C(1)–P(1)–Cu(1) 111.33(18), Cu(1)–P(1)–C(20) 121.7(2), P(1)–Cu(1)–Br(2) 130.81(5), P(1)–Cu(1)–Br(3) 127.82(5), Cu(1)–Br(2)–Cu(2) 78.64(3).

Catalysis

Complexes **7**–**12** were then used to explore their catalytic activity in the CO_2-fixation of terminal alkynes as outlined in the introduction. In this investigation, the carboxylation of phenylacetylene was selected as a model reaction to study the influence of various ligands on catalysis compared with CuI, CuBr and $Cu(MeCN)_4BF_4$.

As shown in Fig. 9, complexes **7**–**12** exhibited a higher catalytic activity compared to the free copper salts. The maximum increase of such catalytic activity can be seen for the Cu $(MeCN)_nBF_4$ analogues, where the yield increased from 29% for $Cu(MeCN)_4BF_4$ to 59% and 76% for complexes **9** and **12**, respectively (entries 3, 6, and 9, Table 1 and Fig. 9). However, the catalytic activity of such complexes over the simple Cu halide decreases as the size of the halide increases [CuBr salts: 41% for CuBr to 62% for **7** and 88% for **10** (entries 2, 4 and 7, Table 1 and Fig. 9); CuI salts: 58% for CuI to 69% for **8** and

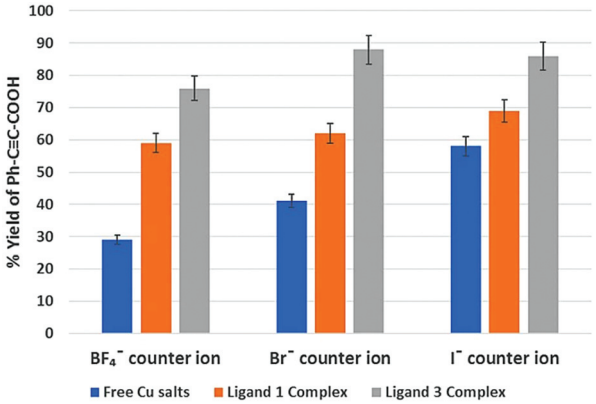

Fig. 9 Catalytic efficiency for the carboxylation reaction of Ph–C≡CH to form Ph–C≡C–COOH. The blue, orange and grey bars show the yields resulting from free copper salts, and the corresponding Cu(I) complexes with ligands **1** and **3**, respectively. As the yields listed here are the averages of two consecutive catalytic reactions, error bars of 5% are shown for all yields.

Table 1 Survey of catalytic activity in the formation of phenylpropiolic acid from phenylacetylene using 3 mol% of the respective catalysts (*cf.* Table S3† for further details and variations)

Entry	Catalyst	Product yield
1	CuI	58
2	CuBr	41
3	$Cu(MeCN)_4(BF_4)$	29
4	**7**	62
5	**8**	69
6	**9**	59
7	**10**	88
8	**11**	86
9	**12**	76
10	dppf·$Cu(MeCN)_2(BF_4)$	33

86% for **11** (entries 1, 5 and 8, Table 1 and Fig. 9)]. In order to make a fair comparison between dppf and our ligands (*i.e.* **1** and **3**), a similar catalytic reaction was further carried out with dppf·$Cu(MeCN)_2BF_4$ (entry 10, Table 1) as a catalyst, where 33% yield has been obtained, which was slightly higher than that of free $Cu(MeCN)_4BF_4$, but significantly lower than that of **9** and **12** (entries 6 and 9, Table 1). For the sake of completeness, it should be mentioned that CuCl and its respective complexes were not included in this comparison as they showed much lower catalytic conversion (*ca.* 5–10%) under otherwise identical conditions with no significant difference between complexes and free salts.

In general, the catalytic activity of the complexes of phosphane ligands is raised by increasing the steric bulk of the substituents on phosphorus.[21,51] An opposite trend is being noticed in our case, where complexes **10–12** produce higher yields than **7–9** (Table S3, ESI file‡) which may be attributed to the complexation mode observed for ferrocene based ligands where all phosphorus donor sites are mesityl substituted. Complexes **13** and **14** are the only examples for these ligands whose structural information is available and show this feature consistently. Since the conversion of **7** to **13** involves the transfer of CuBr units, it can be speculated that in complexes **7–9** the metal is more loosely bound, due to the high steric bulk of ligand **1**. The lower complex stability of Cu(I) with **1** (in comparison to **3**) was further corroborated by the **7** + **3** → **10** + **1** ligand-exchange reaction, which is slightly exothermic (−4.4 kcal mol^{-1} at the ω-B97X-D/6-311+G**//ω-B97X-D/6-31G* level of theory, Fig. S74 in ESI file‡). To test this hypothesis experimentally, the organic washings of the catalytic reactions were collected, dried under high vacuum, and analyzed by ^{31}P NMR, which revealed that complexes **7–9** dissociate to give free ligand **1** during catalysis (Fig. S55 and S56 in ESI file‡), whereas for complexes **10–12** the Cu–P bonds remain intact (Fig. S57 and S58 in ESI file‡). It should be highlighted that we have further investigated computationally the CO_2 insertion step in the catalytic system, which is usually the rate limiting step.[101,102] The calculated reaction barriers are somewhat lower (by 1.2 kcal mol^{-1} at the ω-B97X-D/6-311+G**//ω-B97X-D/6-31G* level of theory) in the case of the complexes with **3** in comparison to those of **1**, which can also be an explanation for the lower activity of its complexes (see Table S5 in the ESI file‡).

Conclusion

In summary, the tetra- and dimesityl analogues of dppf, **1** and **3** have been synthesized and their ligand properties were explored. The phosphorus lone pairs of tetramesityl substituted **1** show a lower s character, and therefore, a higher donating ability than those in Ph_3P and dppf as indicated by spectroscopic, structural, electrochemical and computational means. In line with these experimental findings, the lone pair at phosphorus makes a significant contribution to the HOMO in **1** and **3**, which explains the cathodic shift of the oxidation potentials with increasing mesityl substitution. For a series of Cu(I) complexes of these ligands, a variety of structural motifs have been found, ranging from the rare double bridging mode over dimeric bridging to isolated Cu-centers. With unsymmetrical ligand **3** stable complexes were formed with isolated Cu (I) centers, while the sterically more challenged tetramesityl substituted **1** is prone to dimeric bridging with increased separation of the phosphorus atoms and its adjacent mesityl substituents. As a consequence of its hemilabile nature, the Cu(I) complexes of **3** showed improved catalytic activity in the addition of CO_2 to terminal alkynes as compared with the respective complexes of **1** which in turn showed superior performance compared to the respective dppf complexes. The potential of these ligands for complexation with other metals and the catalytic activity of these complexes will be explored in the near future.

Experimental section

All manipulations were performed under an argon atmosphere unless mentioned otherwise. Prior to use, glassware was dried

in a drying oven at 120 °C. Solvents were distilled over drying agents, prescribed in the CRC Handbook of Chemistry and subsequently stored under an argon atmosphere over 4 Å molecular sieves. Solvents for column chromatography and aqueous workups were used from bottles (analytical grade supplied by VWR and Alfa-Aesar) without further purification. NMR solvents (purchased from Deutero) were degassed *via* a few cycles of freeze, pump and thaw and finally stored over 3 Å molecular sieves under an argon atmosphere.

Reagents and chemicals were purchased from commercial suppliers (Sigma-Aldrich, ABCR, Alfa-Aesar) and used as received. $Fc'(PCl_2)_2$, $MesLi{\cdot}LiBr{\cdot}OEt_2$, and $dppf{\cdot}Cu(MeCN)_2BF_4$ were synthesized by following the procedure reported in the literature.[56,57,103,104] Mes_2PX (X = Cl/Br, 48%/52%; Fig. S1 and S2 in ESI file‡) was synthesized by following the procedure reported for Xyl_2PX (X = Cl, Br).[105] It should be noted that all the chemical manipulations, involving Mes_2PX as a reagent, require careful calculations of its formula weights. This is because the ^{1}H NMR spectra of Mes_2PX, obtained from different preparation attempts have shown different proportional ratios of Mes_2PCl and Mes_2PBr (*e.g.* 48 : 52 and 53 : 47). Due to minor side reactions, such as unwanted dilithiation and subsequent *in situ* hydrolysis, compounds **3** and **4** contain an impurity, wherein only the dimesitylphosphano group is present on ferrocene. We could not remove this compound from the targeted species and, therefore, used species **3** and **4** contaminated with *ca.* 1–4% of dimesitylphosphanoferrocene for the subsequent chemical transformations (see Fig. S9, S12 and S13 in ESI file‡).

NMR spectra were recorded with Varian 500VNMRS and Varian MR-400 spectrometers at 22 °C. Chemical shifts (δ in ppm) were expressed with respect to the following standards, set as 0 ppm: $SiMe_4$ (for ^{1}H and ^{13}C), aqueous H_3PO_4 (for ^{31}P), $BF_3{\cdot}OEt_2$ (in $CDCl_3$ for ^{11}B) and $CFCl_3$ (for ^{19}F). The signals, resulting from the residual non-deuterated NMR solvents, were locked as indicated in the literature.[106] In addition to the standard notation of signal multiplicity (s = singlet, d = doublet, m = multiplet, dd = doublet of doublet *etc.*), pst, brs, brd and brm were used to abbreviate pseudo-triplet, broad singlet, broad doublet and broad multiplet, respectively. The amount of residual solvents (if present) was verified by NMR analysis and the expected values for elemental analyses were calculated accordingly. The NMR spectra of compounds **1** and **3–6** were recorded in toluene-d8 and thf-d8, and those for the corresponding complexes (**7–12** and **14**) were only recorded either in thf-d8 or CD_3CN. This is because, the complexes could not be dissolved in toluene-d8 by any means. Due to the reason of lower solubility even in the donating solvents (like thf-d8 or CD_3CN), the ^{13}C NMR spectra of some complexes are relatively poor and as a result, signals for the *ipso*-carbons could not be seen after a substantially high number of scans. On the other hand, the diphosphano ferrocene ligands were insoluble in CD_3CN and, therefore, the NMR spectra in the corresponding solvent could not be recorded.

Infrared spectra recorded for the neat substances of **9** and **12** were obtained using a Bruker Alpha Platinum ATR spectrometer, and Opus 6.5 (from Bruker Optics) was used for analysing the data. Strong, medium strong and weak peaks for these species were denoted as s, m and w, respectively. For the sake of comparison, the infrared spectra of $Cu(MeCN)_4BF_4$ and $dppf{\cdot}Cu(MeCN)_2BF_4$ were also recorded under identical conditions for comparison and are depicted in the ESI file (Fig. S75‡). Electrospray ionisation (ESI) and atmospheric pressure chemical ionization (APCI) mass spectra were recorded with a Finnigan LCQ Deca (ThermoQuest, San Jose, USA) instrument using samples dissolved in HPLC-quality thf, and MALDI was recorded with an UltraFlex ToF/ToF (Bruker Daltonics, Bremen, D) instrument, where an N_2 laser with a 337 nm wavelength and 3 ns pulse duration was used. The matrix used for MALDI measurements was DCTB (2-[(2E)-3-(4-*tert*-butylphenyl)-2-methylprop-2-enylidene] malononitrile). Elemental analyses were performed without the presence of any external oxidizer (like V_2O_5) in an EA 3000 Elemental Analyzer (EuroVector). X-ray diffraction experiments were performed using either a STOE IPDS II [using Mo-Kα source (λ = 0.71073 Å)] or a STOE StadiVari [using either an Mo-GENIX source (λ = 0.71073 Å), or a Cu-GENIX source (λ = 1.54186 Å)] diffractometer. Structures were solved using the dual space method (SHELXT) and were refined with SHELXL-2018.[107] All non-hydrogen atoms were refined anisotropically, whereas hydrogen atoms were placed on adjacent atoms using a riding model. Further programs used in the structure analyses were Mercury and Platon.[108–110]

All cyclic voltammetry measurements were carried out in an MBraun acrylic glove box GB2202-C-VAC under an argon atmosphere. Samples were measured as a solution (0.1 M) in dry and deoxygenated CH_2Cl_2, where anhydrous $[Bu_4N][PF_6]$ was used as a conducting salt at a concentration of 0.1 M. The three-electrode cell consisted of a platinum working electrode, a silver counter electrode and a silver pseudoreference electrode. The potential was driven on a WaveDriver 20 Bipotentiostat from the Pine Research Instrument and the electrochemical data were recorded *via* AfterMath (Ver. 1.5.9807, Pine Instrument). All redox processes were referenced using half wave potentials of $(C_5Me_5)_2Fe$ as the standard, which was added to the analyzed solution. Its corresponding value was then subtracted from the recorded potentials to convert them to the Fc/Fc^+ scale following established procedures[111] and then finally evaluated with AfterMath and Excel.

$Fc'(PMes_2)_2$ (1)

A solution of $Fc'(PCl_2)_2$ (0.388 g, 1.00 mmol) in thf (10 mL) was added dropwise to a cold (−84 °C) and stirred suspension of $MesLi{\cdot}LiBr{\cdot}OEt_2$ (1.145 g, 3.99 mmol) in hexanes (100 mL). The reaction mixture was slowly warmed to rt over 3–4 h and stirred for 18 h at rt. After all volatiles were removed under vacuum (10^{-3} mbar), the resulting compound was extracted with toluene (60 mL) and tested by ^{7}Li NMR. A small peak at δ 7.33 ppm in ^{7}Li NMR indicated the presence of soluble LiCl in the crude, which was further evacuated to dryness and extracted with toluene (30 mL). The volume of the thus

obtained toluene solution was reduced to *ca.* 5 mL and finally precipitated on a cold (−20 °C) and vigorously stirred mixture of Et_2O and pentane (40 mL, 1 : 1). The supernatant solution was carefully decanted and the precipitate was dried under high vacuum (10^{-3} mbar), resulting in compound **1** as a pale yellow amorphous solid (70%). Note: this compound has also been synthesized (with a yield of 66%) by the reaction of $FcLi_2{\cdot}(tmeda)_{2/3}$ (1 mmol) and Mes_2PX (X = Cl/Br, 48%/52%, F_W = 327.914 g mol^{-1}, 0.669 g, 2.04 mmol) in thf at −84 °C, with a subsequent workup as mentioned above. ^{1}H NMR (toluene-d8): δ 2.08 (s, 12H, *p*-CH_3 of Mes), 2.31 (s, 24H, *o*-CH_3 of Mes), 4.20 (m, 4H, β-H of Cp), 4.25 (m, 4H, α-H of Cp), 6.66 (brs, 8H, *m*-H of Mes). ^{1}H NMR (thf-d8): δ 2.17 (s, 24H, *o*-CH_3 of Mes), 2.18 (s, 12H, *p*-CH_3 of Mes), 4.19 (m, 4H, β-H of Cp), 4.22 (m, 4H, α-H of Cp), 6.74 (brs, 8H, *m*-H of Mes). ^{13}C{^{1}H} NMR (toluene-d8): δ 21.28 (s, *p*-*C*H$_3$ of Mes), 23.47 (d, *o*-*C*H$_3$ of Mes, J = 15 Hz), 72.50 (d, β-C of Cp, J = 4 Hz), 76.00 (d, α-C of Cp, J = 19 Hz), 80.14 (d, *ipso*-C of Cp, J = 13 Hz), 127.34 (s, *p*-Aryl *C* of Mes), 130.48 (d, *m*-Aryl *C* of Mes, J = 3 Hz), 132.65 (d, *ipso*-Aryl *C* of Mes, J = 21 Hz), 142.53 (d, *o*-Aryl *C* of Mes, J = 15 Hz). ^{13}C{^{1}H} NMR (thf-d8): δ 20.72 (s, *p*-*C*H$_3$ of Mes), 23.29 (d, *o*-*C*H$_3$ of Mes, J = 15 Hz), 72.68 (d, β-C of Cp, J = 4 Hz), 76.24 (d, α-C of Cp, J = 18 Hz), 80.27 (d, *ipso*-C of Cp, J = 13 Hz), 130.52 (d, *p*-Aryl *C* of Mes, J = 4 Hz), 132.82 (d, *ipso*-Aryl *C* of Mes, J = 20 Hz), 137.95 (s, *m*-Aryl *C* of Mes), 142.75 (d, *o*-Aryl *C* of Mes, J = 15 Hz). ^{31}P{^{1}H} NMR (toluene-d8): δ −35.1. ^{31}P{^{1}H} NMR (thf-d8): δ −33.5. MS (APCI-DIP): *m*/*z* (%) 722 (100) $[M]^+$. HRMS (APCI-DIP; *m*/*z*): $[M]^+$ calc. for $C_{46}H_{52}FeP_2$, 722.28937; found 722.28882. Anal. calcd for $C_{46}H_{52}FeP_2$: C, 76.45; H, 7.25. Found: C 75.23; H, 7.16. Probably due to the presence of a little amount of LiCl, the CHN values for this compound differ significantly than expected. As these values could not be improved after several attempts, the purity of the species was further clarified by mass spectrometry (see Fig. S68 in ESI file‡).

Fc′(PMes$_2$)Br (4)

^{n}BuLi (2.5 M in hexanes, 0.84 mL, 2.10 mmol) was added dropwise to a cold (−84 °C) and stirred thf (20 mL) solution of dibromoferrocene (0.687 g, 2.00 mmol). After the gradual color change from pale yellow to bright orange, the solution was stirred at −84 °C for another 30 min. Another solution of Mes_2PX (X = Cl/Br, 48%/52%, F_W = 327.914 g mol^{-1}, 0.679 g, 2.07 mmol) in thf (20 mL) was slowly added to the previous cold solution over 5 min. After warming up to the ambient temperature, the reaction mixture was stirred overnight. All volatiles were removed under high vacuum (10^{-3} mbar) and the product was extracted with hexanes (50 mL). The volume of the filtrate was reduced to *ca.* 10 mL and the almost pure compound was obtained as yellow crystals upon refrigeration at −78 °C. This product had an impurity of dimesitylphosphanoferrocene (*ca.* 5%) which could be reduced to *ca.* 2–3% upon further crystallization in hexanes at −10 °C and the final product was obtained as bright orange crystals (53%). ^{1}H NMR (C_6D_6): δ 2.08 (s, 6H, *p*-CH_3 of Mes), 2.37 (s, 12H, *o*-CH_3 of Mes), 3.85 (pst, 2H, β-H of Cp^{Br}), 4.19 (pst, 2H, α-H of Cp^{Br}), 4.23 (pst, 2H, β-H of Cp^{PMes_2}), 4.32 (m, 2H, α-H of Cp^{PMes_2}), 6.71 (d, 4H, *m*-H of Mes, J = 3 Hz). ^{13}C{^{1}H} NMR (C_6D_6): δ 20.89 (s, *p*-*C*H$_3$ of Mes), 23.51 (d, *o*-*C*H$_3$ of Mes, J = 15 Hz), 69.04 (s, β-C of Cp^{Br}), 71.59 (s, α-C of Cp^{Br}), 74.20 (d, β-C of Cp^{PMes_2}, J = 4 Hz), 77.23 (d, α-C of Cp^{PMes_2}, J = 18 Hz), 78.09 (s, *ipso*-C of Cp^{Br}), 81.55 (d, *ipso*-C of Cp^{PMes_2}, J = 13 Hz), 130.57 (d, *m*-Aryl *C* of Mes, J = 3 Hz), 132.47 (d, *o*-Aryl *C* of Mes, J = 21 Hz), 137.81(s, *p*-Aryl *C* of Mes), 142.57 (d, *ipso*-Aryl *C* of Mes, J = 14 Hz). ^{31}P{^{1}H} NMR (C_6D_6): δ −35.5. MS (APCI-DIP): *m*/*z* (%) 533 (100) $[M]^+$. HRMS (APCI-DIP; *m*/*z*): $[M]^+$ calc. for $C_{28}H_{30}BrFeP$, 533.06179; found 533.069069. Anal. calcd for $C_{28}H_{30}BrFeP$: C, 63.07; H, 5.67. Found: C, 63.32; H, 5.75.

Fc′(PMes$_2$)(PPh$_2$) (3)

^{n}BuLi (2.5 M in hexanes, 0.15 mL, 0.38 mmol) was added dropwise to a cold (0 °C) thf (20 mL) solution of Fc′(PMes$_2$)Br (0.200 g, 0.38 mmol). After the gradual color change from orange to bright red, the solution was stirred at 0 °C for 30 min. Another solution of Ph_2PCl (72 μL, 0.086 g, 0.40 mmol) in hexanes (10 mL) was slowly added to the above cold solution over 5 min. After warming up to the ambient temperature, the reaction mixture was stirred overnight. All volatiles were removed under high vacuum (10^{-3} mbar) and the product was extracted with hexanes (20 mL). The volume of the filtrate was reduced to *ca.* 5 mL and the almost pure compound was obtained as yellow crystals (62%) upon refrigeration at −78 °C. This product had an impurity of dimesitylphosphanoferrocene (*ca.* 3–4%) which could not be reduced upon further crystallization. ^{1}H NMR (toluene-d8): δ 2.08 (s, 6H, *p*-CH_3 of Mes), 2.30 (s, 12H, *o*-CH_3 of Mes), 4.04 (m, 2H, β-H of Cp^{PPh_2}), 4.10 (pst, 2H, α-H of Cp^{PPh_2}), 4.17 (m, 2H, β-H of Cp^{Mes}), 4.21 (pst, 2H, α-H of Cp^{Mes}), 6.66 (brd, 4H, *m*-H of Mes, J = 3 Hz), 7.01–7.02 (m, 6H, *m* and *p*-H of Ph), 7.38 (m, 4H, *o*-H of Ph). ^{1}H NMR (thf-d8): δ 2.16 (s, 12H, *o*-CH_3 of Mes), 2.19 (s, 6H, *p*-CH_3 of Mes), 4.01 (m, 2H, β-H of Cp^{PPh_2}), 4.14 (m, 2H, α-H of Cp^{PPh_2}), 4.18 (m, 2H, β-H of Cp^{Mes}), 4.26 (pst, 2H, α-H of Cp^{Mes}), 6.74 (brd, 4H, *m*-H of Mes, J = 3 Hz), 7.23–7.29 (m, 10H, *o*, *m* and *p*-H of Ph). ^{13}C{^{1}H} NMR (toluene-d8): δ 20.87 (s, *p*-*C*H$_3$ of Mes), 23.47 (d, *o*-*C*H$_3$ of Mes, J = 15 Hz), 72.27 (d, β-C of Cp^{PPh_2}, J = 3 Hz), 72.80 (d, β-C of Cp^{PMes_2}, J = 4 Hz), 74.28 (d, α-C of Cp^{PPh_2}, J = 15 Hz), 75.86 (d, α-C of Cp^{PMes_2}, J = 18 Hz), 77.34 (d, *ipso*-C of Cp^{PPh_2}, J = 10 Hz), 80.57 (d, *ipso*-C of Cp^{PMes_2}, J = 13 Hz), 128.34 (d, *m*-Aryl *C* of Ph, J = 7 Hz), 128.57 (s, *p*-Aryl *C* of Ph), 130.49 (d, *m*-Aryl *C* of Mes, J = 3 Hz), 132.61 (d, *o*-Aryl *C* of Mes, J = 21 Hz), 133.92 (d, *o*-Aryl *C* of Ph, J = 21 Hz), 140.05 (d, *ipso*-Aryl *C* of Ph, J = 15 Hz), 142.54 (d, *ipso*-Aryl *C* of Mes, J = 15 Hz). ^{13}C{^{1}H} NMR (thf-d8): δ 20.90 (s, *p*-*C*H$_3$ of Mes), 23.48 (d, *o*-*C*H$_3$ of Mes, J = 15 Hz), 72.68 (dd, β-C of Cp^{PPh_2}, J = 4, 1 Hz), 73.11 (d, β-C of Cp^{PMes_2}, J = 4 Hz), 74.63 (d, α-C of Cp^{PPh_2}, J = 15 Hz), 76.28 (d, α-C of Cp^{PMes_2}, J = 18 Hz), 77.71 (d, *ipso*-C of Cp^{PPh_2}, J = 10 Hz), 80.81 (d, *ipso*-C of Cp^{PMes_2}, J = 13 Hz), 128.78 (d, *m*-Aryl *C* of Ph, J = 7 Hz), 129.09 (s, *p*-Aryl *C* of Ph), 130.70 (d, *m*-Aryl *C* of Mes, J = 3 Hz), 132.95 (d, *o*-Aryl *C* of Mes, J = 21 Hz), 134.27 (d, *o*-Aryl *C* of Ph, J = 20 Hz), 138.11 (s, *p*-Aryl *C* of Mes), 140.43 (d, *ipso*-Aryl *C* of Ph, J = 11 Hz), 142.91 (d, *ipso*-Aryl *C* of Mes, J = 15 Hz). ^{31}P{^{1}H} NMR

(toluene-d8): δ −34.8 (*P*Mes$_2$), −17.0 (*P*Ph$_2$). ^{31}P{^{1}H} NMR (thf-d8): δ −35.1 (*P*Mes$_2$), −17.2 (*P*Ph$_2$). MS (APCI-DIP): *m*/*z* (%) 639 [M + 1]$^+$. HRMS (APCI-DIP; *m*/*z*): [M + 1]$^+$ calc. for $C_{40}H_{40}FeP_2$, 639.19547; found 639.20281. Anal. calcd for $C_{40}H_{40}FeP_2$: C, 75.24; H, 6.31. Found: C, 74.92; H, 6.45.

Diselenide derivatives of 1 and 3

A suspension of red Se (0.120 g, 1.52 mmol) and **1** (0.170 g, 0.24 mmol) or **3** (0.153 g, 0.24 mmol) in thf (20 mL) was stirred for 1 h at r.t. All volatiles were removed under high vacuum (10^{-3} mbar) and the product was extracted with hot toluene. The analytically pure compound was crystallized from the hot toluene solution by slow cooling up to ambient temperature. Note: if all residual Se is not removed by single filtration, the procedure of filtration must be repeated multiple times before crystallization.

Fc′(PSeMes$_2$)$_2$ (5)

Yield: 67%. ^{1}H NMR (toluene-d8): δ 1.99 (s, 12H, *p*-C*H*$_3$ of Mes), 2.38 (brs, 24H, *o*-C*H*$_3$ of Mes), 4.79 (m, 4H, Cp), 4.90 (brs, 4H, Cp), 6.52 (m, 8H, *m*-H of Mes). ^{13}C{^{1}H} NMR (toluene-d8): δ 24.43 (d, *o*-*C*H$_3$ of Mes, *J* = 6 Hz), 75.72 (d, β-C of Cp, *J* = 9 Hz), 78.25 (brs, α-C of Cp), 82.45 (d, *ipso*-C of Cp, *J* = 78 Hz), 125.63 (s, *p*-Aryl *C* of Mes), 132.15 (d, *o*-Aryl *C* of Mes, *J* = 11 Hz), 139.72 (d, *m*-Aryl *C* of Mes, *J* = 2 Hz), 140.49 (brm, *ipso*-Aryl *C* of Mes). ^{31}P{^{1}H} NMR (toluene-d8): δ 14.7 ($^1J_{P,Se}$ = 723 Hz). ^{77}Se{^{1}H} NMR (toluene-d8): δ −82.6 (P*Se*Mes$_2$, $^1J_{P,Se}$ = 723 Hz). MS (MALDI): *m*/*z* (%) 880 (100) [M]$^+$. Anal. calcd for $C_{46}H_{52}FeP_2Se_2$: C, 62.74; H, 5.95. Found: C, 62.89; H, 5.90.

Fc′(PSeMes$_2$)(PSePh$_2$) (6)

Yield: 65%. ^{1}H NMR (toluene-d8): δ 1.99 (s, 6H, *p*-C*H*$_3$ of Mes), 2.35 (brs, 12H, *o*-C*H*$_3$ of Mes), 4.42 (brs, 2H, β-H of Cp^{PPh_2}), 4.69 (brs, 2H, α-H of Cp^{PPh_2}), 4.73 (brs, 2H, α-H of Cp^{Mes}), 4.76 (brs, 2H, β-H of Cp^{Mes}), 6.49 (brd, 4H, *m*-H of Mes, *J* = 4 Hz), 6.92–6.94 (m, 6H, *m* and *p*-H of Ph), 7.70 (m, 4H, *o*-H of Ph). ^{13}C{^{1}H} NMR (toluene-d8): δ 20.69 (d, *p*-*C*H$_3$ of Mes, *J* = 2 Hz), 24.32 (d, *o*-*C*H$_3$ of Mes, *J* = 6 Hz), 74.94 (d, β-C of Cp^{PPh_2}, *J* = 12 Hz), 75.38 (d, α-C of Cp^{PPh_2}, *J* = 9 Hz), 75.99 (d, *ipso*-C of Cp^{PPh_2}, *J* = 86 Hz), 76.12 (d, β-C of Cp^{PMes_2}, *J* = 10 Hz), 78.05 (brd, α-C of Cp^{PMes_2}, *J* = 13 Hz), 82.82 (d, *ipso*-C of Cp^{PMes_2}, *J* = 78 Hz), 128.27 (d, *p*-Aryl *C* of Ph, *J* = 3 Hz), 131.10 (d, *m*-Aryl *C* of Ph, *J* = 3 Hz), 132.08 (d, *o*-Aryl *C* of Ph, *J* = 11 Hz), 132.38 (d, *o*-Aryl *C* of Mes, *J* = 11 Hz), 134.34 (d, *ipso*-Aryl *C* of Ph, *J* = 78 Hz), 139.62 (d, *m*-Aryl *C* of Mes, *J* = 3 Hz), 140.39 (brd, *ipso*-Aryl *C* of Mes). ^{31}P{^{1}H} NMR (toluene-d8): δ 14.8 (*P*Mes$_2$, $^1J_{P,Se}$ = 723 Hz), 30.8 (*P*Ph$_2$, $^1J_{P,Se}$ = 763 Hz). ^{77}Se{^{1}H} NMR (toluene-d8): δ −298.8 (P*Se*Ph$_2$, $^1J_{P,Se}$ = 763 Hz), −77.5 (P*Se*Mes$_2$, $^1J_{P,Se}$ = 723 Hz). MS (ESI): *m*/*z* (%) 797 (100) [M + 1]$^+$. HRMS (ESI; *m*/*z*): [M + 1]$^+$ calc. for $C_{40}H_{40}FeP_2Se_2$, 799.02851; found 799.03579. Anal. calcd for $C_{40}H_{40}FeP_2Se_2$: C, 60.32; H, 5.06. Found: C, 60.44; H, 5.17.

Copper complexes of 1

A suspension of **1** (0.144 g, 0.20 mmol), CuX (0.20 mmol), toluene (10 mL), thf (10 mL) and CH_3CN (2 mL) was refluxed for 24 h. After removal of all insoluble materials by filtration, the volume of the filtrate was reduced to *ca.* 15 mL and analytically pure crystalline or semi-crystalline materials were obtained by slow introduction of dry pentane and kept in a double arm H-tube at ambient temperature. For all compounds, mentioned under this section, the mass spectrometric measurements gave similar data, where the corresponding peak for Fc′(PMes$_2$)$_2$Cu$^+$ was identified as a molecular ion peak. One example is shown in the following: MS (ESI): *m*/*z* (%) 787 [M + 1]$^+$. HRMS (ESI; *m*/*z*): [M]$^+$ calc. for $C_{46}H_{52}CuFeP_2$, 785.21897; found 785.21842.

Fc′(PMes$_2$)$_2$·CuBr (7)

Yield: 63%. ^{1}H NMR (thf-d8): δ 2.00–2.50 (brs, 36H, *o*- and *p*-C*H*$_3$ of Mes), 4.24 (brs overlapped with another brs, 8H, α- and β-H of Cp), 6.79 (brs, 8H, *m*-H of Mes). ^{13}C{^{1}H} NMR (thf-d8): δ 20.88 (brs, *p*-*C*H$_3$ of Mes), 73.12 (brs, α- and β-H of Cp), 78.46 (brs, *ipso*-C of Cp), 126.01 (s, *p*-Aryl *C* of Mes), 128.88 (s, *m*-Aryl *C* of Mes), 129.64 (s, *o*-Aryl *C* of Mes), 131.52 (brs, *ipso*-Aryl *C* of Mes). ^{31}P{^{1}H} NMR (thf-d8): δ −26.8. Anal. calcd for $C_{46}H_{52}BrCuFeP_2$: C, 63.79; H, 6.05. Found: C, 63.72; H, 5.88.

Fc′(PMes$_2$)$_2$·CuI (8)

Yield: 58%. ^{1}H NMR (thf-d8): δ 2.00–2.50 (brs, 36H, *o*- and *p*-C*H*$_3$ of Mes), 4.27 (brs overlapped with another brs, 8H, α- and β-H of Cp), 6.83 (brs, 8H, *m*-H of Mes). ^{13}C{^{1}H} NMR (thf-d8): δ 20.87 (brs, *p*-*C*H$_3$ of Mes), 72.72 (brs, α- and β-H of Cp), 126.01 (s, *p*-Aryl *C* of Mes), 128.88 (s, *m*-Aryl *C* of Mes), 129.64 (s, *o*-Aryl *C* of Mes), 131.52 (brs, *ipso*-Aryl *C* of Mes). ^{31}P{^{1}H} NMR (thf-d8): δ −25.0. Anal. calcd for $C_{46}H_{52}CuFeIP_2$: C, 60.50; H, 5.74. Found: C, 60.72; H, 5.35.

Fc′(PMes$_2$)$_2$·Cu(BF$_4$) (9)

Yield: 69%. ^{1}H NMR (CD_3CN): δ 2.00–2.50 (brs, 36H, *o*- and *p*-C*H*$_3$ of Mes), 4.24 (brs, 4H, β-H of Cp), 4.45 (brs, 4H, α-H of Cp), 6.91 (brs, 8H, *m*-H of Mes). ^{13}C{^{1}H} NMR (CD_3CN): δ 20.82 (s, *p*-*C*H$_3$ of Mes), 24.98 (brs, *o*-*C*H$_3$ of Mes), 73.47 (brs, α- and β-H of Cp), 78.70 (t, *ipso*-H of Cp, *J* = 17 Hz), 126.21 (s, *p*-Aryl *C* of Mes), 129.18 (s, *m*-Aryl *C* of Mes), 129.87 (s, *o*-Aryl *C* of Mes), 131.89 (brs, *ipso*-Aryl *C* of Mes). ^{31}P{^{1}H} NMR (CD_3CN): δ −27.8. ^{11}B{^{1}H} NMR (CD_3CN): δ −1.2. ^{19}F{^{1}H} NMR (CD_3CN): δ −151.9. IR (ATR) ν: 1024 (m), 1159 (m), 1444 (m), 1466 (m), 1602 (w), 2918 (w). Anal. calcd for $C_{46}H_{52}BCuF_4FeP_2$: C, 63.28; H, 6.00. Found: C, 63.25; H, 6.01.

Copper complexes of 3

A suspension of **3** (0.128 g, 0.20 mmol), CuX (0.2 mmol), toluene (10 mL), thf (10 mL) and CH_3CN (2 mL) was refluxed for 24 h. After removal of all insoluble materials by filtration, the volume of the filtrate was reduced to *ca.* 15 mL and analytically pure crystalline or semi-crystalline materials were obtained by slow evaporation under an inert atmosphere at ambient temperature. For all compounds, mentioned under this section, the mass spectrometric measurements gave similar data, where the corresponding peak for Fc′(PMes$_2$)(PPh$_2$)Cu$^+$ was identified as a molecular ion peak. One

example is shown in the following: MS (ESI): *m*/*z* (%) 701 $[M]^+$. HRMS (ESI; *m*/*z*): $[M]^+$ calc. for $C_{40}H_{40}CuFeP_2$, 701.12507; found 701.12452.

$Fc'(PMes_2)(PPh_2)\cdot CuBr$ (10)

Yield: 71%. ^{1}H NMR (thf-d8): δ 2.22 (s, 6H, *p*-CH_3 of Mes), 2.32 (s, 12H, *o*-CH_3 of Mes), 4.14 (s, 2H, β-H of Cp^{PPh_2}), 4.27 (pst, 2H, β-H of Cp^{PMes_2}), 4.42 (s, 4H, α-H of Cp^{PPh_2}), 4.49 (brs, 4H, α-H of Cp^{PMes_2}), 6.82 (brm, 4H, *m*-H of Mes), 7.38 (m, 6H, *m* and *p*-H of Ph), 7.92 (m, 4H, *o*-H of Ph). $^{13}C\{^1H\}$ NMR (thf-d8): δ 20.67 (s, *p*-*C*H_3 of Mes), 30.46 (s, *o*-*C*H_3 of Mes), 72.69 (s, β-C of $Cp^{PPh_2,PMes_2}$), 74.48 (s, α-C of Cp^{PPh_2}), 77.41 (s, α-C of Cp^{PMes_2}), 129.12 (d, *p*-Aryl *C* of Ph, J = 10 Hz), 130.67 (s, *m*-Aryl *C* of Ph), 131.63 (s, *m*-Aryl *C* of Mes), 134.95 (d, *p*-Aryl *C* of Mes, J = 15 Hz), 139.66 (s, *o*-Aryl *C* of Ph), 142.92 (s, *o*-Aryl *C* of Mes). $^{31}P\{^1H\}$ NMR (thf-d8): δ −31.5 (d, *P*Mes_2, J = 135 Hz), −19.3 (d, *P*Ph_2, J = 135 Hz). Anal. calcd for $C_{40}H_{40}BrCuFeP_2$: C, 61.44; H, 5.16. Found: C, 61.04; H, 5.15.

$Fc'(PMes_2)(PPh_2)\cdot CuI$ (11)

Yield: 74%. ^{1}H NMR (thf-d8): δ 2.22 (s, 6H, *p*-CH_3 of Mes), 2.29 (s, 12H, *o*-CH_3 of Mes), 4.12 (pst, 2H, β-H of Cp^{PPh_2}), 4.26 (pst, 2H, β-H of Cp^{PMes_2}), 4.42 (s, 4H, α-H of Cp^{PPh_2}), 4.52 (brs, 4H, α-H of Cp^{PMes_2}), 6.82 (d, 4H, *m*-H of Mes, J = 3 Hz), 7.39 (m, 6H, *m* and *p*-H of Ph), 7.92 (m, 4H, *o*-H of Ph). $^{13}C\{^1H\}$ NMR (thf-d8): δ 20.85 (s, *p*-*C*H_3 of Mes), 24.75 (dd, *o*-*C*H_3 of Mes, J = 9 and 1 Hz), 72.91 (m, β-C of $Cp^{PPh_2,PMes_2}$), 74.82 (d, α-C of Cp^{PPh_2}, J = 10 Hz), 77.59 (m, α-C of Cp^{PMes_2}), 129.28 (d, *p*-Aryl *C* of Ph, J = 10 Hz), 130.88 (m, *m*-Aryl *C* of Ph), 131.83 (d, *m*-Aryl *C* of Mes, J = 6 Hz), 135.20 (d, *p*-Aryl *C* of Mes, J = 15 Hz), 139.86 (s, *o*-Aryl *C* of Ph), 142.94 (d, *o*-Aryl *C* of Mes, J = 11 Hz). $^{31}P\{^1H\}$ NMR (thf-d8): δ −30.1 (brm, *P*Mes_2), −20.2 (d, *P*Ph_2, J = 98 Hz). Anal. calcd for $C_{40}H_{40}CuFeIP_2$: C, 57.95; H, 4.86. Found: C, 57.66; H, 4.90.

$Fc'(PMes_2)(PPh_2)\cdot Cu(MeCN)_2(BF_4)$ (12)

Yield: 77%. ^{1}H NMR (thf-d8): δ 2.08 (s, 6H, CH_3 of MeCN) 2.23 (s, 6H, *p*-CH_3 of Mes), 2.30 (s, 12H, *o*-CH_3 of Mes), 4.11 (m, 2H, β-H of Cp^{PPh_2}), 4.32 (pst, 2H, β-H of Cp^{PMes_2}), 4.54 (pst, 4H, α-H of Cp^{PPh_2}), 4.63 (pst, 4H, α-H of Cp^{PMes_2}), 6.90 (, 4H, *m*-H of Mes), 7.48 (m, 6H, *m* and *p*-H of Ph), 7.68 (m, 4H, *o*-H of Ph). $^{13}C\{^1H\}$ NMR (thf-d8): δ 1.16 (s, *C*H_3CN), 20.84 (s, *p*-*C*H_3 of Mes), 24.45 (dd, *o*-*C*H_3 of Mes, J = 11 and 1 Hz), 73.27 (d, β-C of Cp^{PPh_2}, J = 5 Hz), 73.61 (d, β-C of Cp^{PMes_2}, J = 6 Hz), 74.62 (d, α-C of Cp^{PPh_2}, J = 9 Hz), 75.25 (d, *ipso*-C of Cp^{PPh_2}, J = 47 Hz), 77.71 (d, α-C of Cp^{PMes_2}, J = 14 Hz), 78.94 (d, *ipso*-C of Cp^{PMes_2}, J = 39 Hz), 119.76 (s, CH_3CN), 126.06 (dd, *ipso*-C of Ph, J = 28 and 3 Hz), 130.08 (d, *p*-Aryl C of Ph, J = 10 Hz), 131.57 (d, *m*-Aryl C of Ph, J = 2 Hz), 132.02 (d, *p*-Aryl *C* of Mes, J = 7 Hz), 133.34 (d, *ipso*-C of Mes, J = 31 Hz), 134.70 (d, *o*-Aryl *C* of Ph, J = 16 Hz), 140.61 (d, *m*-Aryl *C* of Mes, J 2 = Hz), 142.94 (d, *o*-Aryl *C* of Mes, J = 11 Hz). $^{31}P\{^1H\}$ NMR (thf-d8): δ −33.5 (d, *P*Mes_2, J = 119 Hz), −11.8 (d, *P*Ph_2, J = 119 Hz). $^{11}B\{^1H\}$ NMR (thf-d8): δ −0.9. $^{19}F\{^1H\}$ NMR (thf-d8): δ −153.2. IR (ATR) ν: 1025 (s), 1034 (s), 1053 (s), 1093 (m), 1436 (m), 1600 (w), 2228 (w), 2922 (w). Anal. calcd for $C_{44}H_{46}BCuF_4FeN_2P_2$: C, 60.67; H, 5.32; N, 3.22. Found: C, 60.45; H, 5.34; N, 2.96.

$[Fc'(PMes_2)_2\cdot(CuBr)_2]_2$ (13)

A suspension of **1** (0.144 g, 0.20 mmol), CuBr (0.057 g, 0.40 mmol), toluene (10 mL), thf (15 mL) and CH_3CN (5 mL) was refluxed for 48 h. After the removal of all insoluble materials by filtration, the volume of the filtrate was reduced to *ca.* 20 mL and the crystalline substances along with the semi-crystalline materials were obtained by slow introduction of dry pentane and kept in a double arm H-tube at ambient temperature. After washing several times with a mixture of dry toluene and pentane (1 : 1), followed by the removal of all volatiles under high vacuum (10^{-3} mbar), compound **13** was obtained in a yield of 56%. ^{1}H NMR (CD_3CN): δ 2.00–2.50 (brs overlapped with another brs, 72H, *o*- and *p*-CH_3 of Mes), 4.25 (brs, 8H, α-H of Cp), 4.60 (brs, 8H, β-H of Cp), 6.88 (brs, 16H, *m*-H of Mes). $^{31}P\{^1H\}$ NMR (thf-d8): δ −26.9. $^{31}P\{^1H\}$ NMR (CD_3CN): δ −27.5. MS (MALDI): *m*/*z* (%) 850 $[M]^+$ for $[Fc'(PMes_2)_2\cdot Cu_2]^{2+}$, 786 $[M]^+$ for $[Fc'(PMes_2)_2\cdot Cu]^+$. Anal. calcd for $C_{46}H_{52}BrCuFeP_2$: C, 54.72; H, 5.19. Found: C, 54.59; H, 5.06. Note: compound **13** is highly insoluble in commonly available organic solvents (including thf-d8 and CD_3CN). After a prolonged NMR experiment only ^{1}H (with a low S/N ratio and unresolved broad signals near the baseline) and $^{31}P\{^1H\}$ NMR spectra (with a satisfactory S/N ratio) could be obtained, which revealed the absence of any starting ligand (**1**) in the resulting mixture.

$[Fc'(PMes_2)Br\cdot CuBr]_2$ (14)

A suspension of **4** (0.107 g, 0.20 mmol), CuBr (0.029 g, 0.20 mmol), toluene (10 mL), thf (10 mL) and CH_3CN (2 mL) was refluxed for 24 h. After the removal of all insoluble materials by filtration, the volume of the filtrate was reduced to *ca.* 15 mL and analytically pure crystalline materials (72%) were obtained by slow evaporation under an inert atmosphere. ^{1}H NMR (thf-d8): δ 2.22 (brs, 12H, *p*-CH_3 of Mes), 2.29 (brs, 12H, *o*-CH_3 of Mes), 4.19 (pst, 2H, β-H of Cp^{PMes_2}), 4.32 (pst, 2H, β-H of Cp^{Br}), 4.51 (s, 2H, α-H of Cp^{Br}), 4.77 (s, 2H, α-H of Cp^{PMes_2}), 6.83 (d, 8H, *m*-H of Mes, J = 5 Hz). $^{13}C\{^1H\}$ NMR (thf-d8): 20.87(s, *p*-*C*H_3 of Mes), 24.77 (s, *o*-*C*H_3 of Mes), 70.76 (s, β-C of Cp^{Br}), 72.48 (s, α-C of Cp^{Br}), 76.10 (d, β-C of Cp^{PMes_2}, J = 7 Hz), 77.96 (d, *ipso*-C of Cp^{PMes_2}, J = 41 Hz), 78.41 (s, *ipso*-C of Cp^{Br}), 79.09 (brd, α-C of Cp^{PMes_2}), 128.79 (d, *ipso*-Aryl *C* of Mes, J = 36 Hz), 131.74 (d, *p*-Aryl *C* of Mes, J = 7 Hz), 139.97 (s, *m*-Aryl *C* of Mes), 142.11 (d, *o*-Aryl *C* of Mes, J = 11 Hz). $^{31}P\{^1H\}$ NMR (thf-d8): δ −26.5. MS (MALDI and APCI): *m*/*z* (%) 532 (100) $[M]^+$ for the starting ligand $Fc'(PMes_2)Br$ and no peak for its corresponding CuBr complex **14** could be found. Anal. calcd for $C_{56}H_{60}Br_4Cu_2Fe_2P_2$: C, 49.70; H, 4.47. Found: C, 49.99; H, 4.43.

Catalytic reaction

A mixture of Ph–C≡C–H (0.204 g, 0.22 mL, 2 mmol, 1 equiv.), the respective catalyst (mole% with respect to Cu, mentioned in Table S3, ESI file‡), dry DMF (10 mL), and Cs_2CO_3 (0.978 g,

3 mmol, 1.5 equiv.) was degassed by three consecutive cycles of freeze (at −98 °C, MeOH and liquid N_2), pump and thaw. A balloon, filled with dry CO_2, was placed on it and the resulting reaction mixture was stirred for 36 h at rt, followed by quenching with water (20 mL). The organic layer was then separated by washing with DCM (3 × 20 mL) and the combined DCM phases were stored for further investigation. The aqueous layer was acidified with conc. HCl (up to pH 1) and extracted with EtOAc (3 × 20 mL). The resulting EtOAc phases were combined and the residual DMF was removed by washing with water (2 × 30 mL) and brine (30 mL), followed by drying upon anhydrous Na_2SO_4. Volatiles were removed using a rotatory evaporator and the resulting colourless oil was subjected to controlled vacuum (5×10^{-2} mbar), until colourless crystals formed (see Fig. S54 in ESI file‡). The previously collected DCM phase was then washed with water (2 × 30 mL) and brine (30 mL), dried under a rotatory evaporator and finally subjected to high vacuum (10^{-3} mbar) overnight at 40 °C. The thus-obtained yellow solids were then characterized by ^{31}P NMR, which revealed them as the remnants of catalysts.

Conflicts of interest

There are no conflicts to declare.

Acknowledgements

The authors would like to thank the funding programs LOEWE and MASH for financial support. Zsolt Kelemen is grateful for the general support of Hungarian Academy of Science under the Premium Postdoctoral Research Program 2019.

References

1 D. E. Herbert, U. F. Mayer and I. Manners, *Angew. Chem., Int. Ed.*, 2007, **46**, 5060.
2 V. Bellas and M. Rehahn, *Angew. Chem., Int. Ed.*, 2007, **46**, 5082.
3 A. Alkan, L. Thomi, T. Gleede and F. R. Wurm, *Polym. Chem.*, 2015, **6**, 3617.
4 R. Pietschnig, *Chem. Soc. Rev.*, 2016, **45**, 5216.
5 L. Cao, I. Manners and M. A. Winnik, *Macromolecules*, 2002, **35**, 8258.
6 M. Saleem, H. Yu, L. Wang, A. Zain ul, H. Khalid, M. Akram, N. M. Abbasi and J. Huang, *Anal. Chim. Acta*, 2015, **876**, 9.
7 X. Sui, X. Feng, M. A. Hempenius and G. J. Vancso, *J. Mater. Chem. B*, 2013, **1**, 1658.
8 J. Elbert, J. Mersini, N. Vilbrandt, C. Lederle, M. Kraska, M. Gallei, B. Stühn, H. Plenio and M. Rehahn, *Macromolecules*, 2013, **46**, 4255.
9 C. Ornelas, *New J. Chem.*, 2011, **35**, 1973.
10 G. Jaouen, A. Vessieres and S. Top, *Chem. Soc. Rev.*, 2015, **44**, 8802.
11 R. L. Hailes, A. M. Oliver, J. Gwyther, G. R. Whittell and I. Manners, *Chem. Soc. Rev.*, 2016, **45**, 5358.
12 S. Takahashi and J. I. Anzai, *Materials*, 2013, **6**, 5742.
13 P. Debroy and S. Roy, *Coord. Chem. Rev.*, 2007, **251**, 203.
14 D. P. Puzzo, A. C. Arsenault, I. Manners and G. A. Ozin, *Angew. Chem., Int. Ed.*, 2009, **48**, 943.
15 K.-S. Gan and T. S. A. Hor, in *Ferrocenes: Homogeneous Catalysis, Organic Synthesis, Materials Science*, ed. A. Togni and T. Hayashi, John Wiley & Sons, 2007, pp. 3–104.
16 S. W. Chien and T. S. Andy Hor, in *Ferrocenes: Ligands, Materials and Biomolecules*, ed. P. Štěpnička, John Wiley & Sons, 2008, pp. 33–116.
17 J. J. Bishop, A. Davison, M. L. Katcher, D. W. Lichtenberg, R. E. Merrill and J. C. Smart, *J. Organomet. Chem.*, 1971, **27**, 241.
18 G. M. Whitesides, J. F. Gaasch and E. R. Stedronsky, *J. Am. Chem. Soc.*, 1972, **94**, 5258.
19 L. E. Hagopian, A. N. Campbell, J. A. Golen, A. L. Rheingold and C. Nataro, *J. Organomet. Chem.*, 2006, **691**, 4890.
20 G. Bandoli and A. Dolmella, *Coord. Chem. Rev.*, 2000, **209**, 161.
21 M. N. Birkholz, Z. Freixa and P. W. van Leeuwen, *Chem. Soc. Rev.*, 2009, **38**, 1099.
22 P. Dierkes and P. W. N. M. van Leeuwen, *J. Chem. Soc., Dalton Trans.*, 1999, 1519.
23 S. P. Thomas and J. Colacot, in *Ferrocenes: Ligands, Materials and Biomolecules*, ed. P. Štěpnička, John Wiley & Sons, 2008, pp. 117–140.
24 A. Fihri, P. Meunier and J.-C. Hierso, *Coord. Chem. Rev.*, 2007, **251**, 2017.
25 P. Vosáhlo, I. Císařová and P. Štěpnička, *J. Organomet. Chem.*, 2018, **860**, 14.
26 K. Skoch, I. Cisarova, J. Schulz, U. Siemeling and P. Stepnicka, *Dalton Trans.*, 2017, **46**, 10339.
27 P. Štěpnička, in *Ferrocenes: Ligands, Materials and Biomolecules*, ed. P. Štěpnička, John Wiley & Sons, 2008, pp. 177–204.
28 H.-U. Blaser, W. Chen, F. Camponovo and A. Togni, in *Ferrocenes: Ligands, Materials and Biomolecules*, ed. P. Štěpnička, John Wiley & Sons, 2008, pp. 205–235.
29 P. Štěpnička and M. Lamač, in *Ferrocenes: Ligands, Materials and Biomolecules*, ed. P. Štěpnička, John Wiley & Sons, 2008, pp. 237–277.
30 U. Siemeling, in *Ferrocenes: Ligands, Materials and Biomolecules*, ed. P. Štěpnička, John Wiley & Sons, 2008, pp. 141–176.
31 A. L. Boyes, I. R. Butler and S. C. Quayle, *Tetrahedron Lett.*, 1998, **39**, 7763.
32 W. R. Cullen, T. J. Kim, F. W. B. Einstein and T. Jones, *Organometallics*, 1983, **2**, 714.
33 B. C. Hamann and J. F. Hartwig, *J. Am. Chem. Soc.*, 1998, **120**, 3694.
34 O. V. Gusev, T. y. A. Peganova, A. M. Kalsin, N. V. Vologdin, P. V. Petrovskii, K. A. Lyssenko, A. V. Tsvetkov and I. P. Beletskaya, *Organometallics*, 2006, **25**, 2750.

35 I. R. Butler, W. R. Cullen, T. J. Kim, S. J. Rettig and J. Trotter, *Organometallics*, 1985, **4**, 972.
36 T. Y. Dong and C. K. Chang, *J. Chin. Chem. Soc.*, 1998, **45**, 577.
37 A. Fihri, J. C. Hierso, A. Vion, D. H. Nguyen, M. Urrutigoïty, P. Kalck, R. Amardeil and P. Meunier, *Adv. Synth. Catal.*, 2005, **347**, 1198.
38 M. Yamashita, J. V. Cuevas-Vicario and J. F. Hartwig, *J. Am. Chem. Soc.*, 2003, **125**, 16347.
39 J. C. Hierso, F. Lacassin, R. Broussier, R. Amardeil and P. Meunier, *J. Organomet. Chem.*, 2004, **689**, 766.
40 M. Laly, R. Broussier and B. Gautheron, *Tetrahedron Lett.*, 2000, **41**, 1183.
41 T. J. Colacot and H. A. Shea, *Org. Lett.*, 2004, **6**, 3731.
42 G. A. Grasa and T. J. Colacot, *Org. Lett.*, 2007, **9**, 5489.
43 T. R. Kegl, N. Palinkas, L. Kollar and T. Kegl, *Molecules*, 2018, **23**, 3176.
44 G. Cavinato and L. Toniolo, *Molecules*, 2014, **19**, 15116.
45 I. R. Butler, W. R. Cullens and T.-J. Kim, *Synth. React. Inorg. Met.-Org. Chem.*, 2006, **15**, 109.
46 L. Qin, X. Ren, Y. Lu, Y. Li and J. Zhou, *Angew. Chem., Int. Ed.*, 2012, **51**, 5915.
47 M. Ogasawara, K.-i. Takizawa and T. Hayashi, *Organometallics*, 2002, **21**, 4853.
48 L. A. Evans, N. Fey, J. N. Harvey, D. Hose, G. C. Lloyd-Jones, P. Murray, A. G. Orpen, R. Osborne, G. J. J. Owen-Smith and M. Purdie, *J. Am. Chem. Soc.*, 2008, **130**, 14471.
49 Y. Fukue, S. Oi and Y. Inoue, *J. Chem. Soc., Chem. Commun.*, 1994, 2091.
50 S. Wang, G. Du and C. Xi, *Org. Biomol. Chem.*, 2016, **14**, 3666.
51 M. Trivedi, G. Singh, A. Kumar and N. P. Rath, *Dalton Trans.*, 2015, **44**, 20874.
52 L. J. Gooßen, N. Rodríguez, F. Manjolinho and P. P. Lange, *Adv. Synth. Catal.*, 2010, **352**, 2913.
53 W. H. Wang, L. Jia, X. Feng, D. Fang, H. Guo and M. Bao, *Asian J. Org. Chem.*, 2019, **8**, 1501.
54 R. Sihler, U. Werz and H.-A. Brune, *J. Organomet. Chem.*, 1989, **368**, 213.
55 J. Roger, S. Royer, H. Cattey, A. Savateev, R. V. Smaliy, A. N. Kostyuk and J. C. Hierso, *Eur. J. Inorg. Chem.*, 2017, 330.
56 I. E. Nifant'ev, A. A. Boricenko, L. F. Manzhukova and E. E. Nifant'ev, *Phosphorus, Sulfur Silicon Relat. Elem.*, 1992, **68**, 99.
57 C. Moser, A. Orthaber, M. Nieger, F. Belaj and R. Pietschnig, *Dalton Trans.*, 2006, 3879.
58 S. Dey, J. W. Quail and J. Müller, *Organometallics*, 2015, **34**, 3039.
59 M. N. Chevykalova, *Russ. Chem. Bull., Int. Ed.*, 2003, **52**, 78.
60 A. Orthaber, M. Fuchs, F. Belaj, G. N. Rechberger, C. O. Kappe and R. Pietschnig, *Eur. J. Inorg. Chem.*, 2011, 2588.
61 H. Zahra and R. Ali, *Curr. Org. Chem.*, 2018, **22**, 1589.
62 H. Schmidbaur and A. Schier, *Angew. Chem., Int. Ed.*, 2013, **52**, 176.
63 G. J. Grant, *Dalton Trans.*, 2012, **41**, 8745.
64 J. Rodrigues, M. G. Jardim, J. Figueira, M. Gouveia, H. Tomás and K. Rissanen, *New J. Chem.*, 2011, **35**, 1938.
65 R. H. Crabtree, in *Iridium Catalysis*, ed. P. G. Andersson, Springer Berlin Heidelberg, 2011, pp. 1–10.
66 Z. Qiu, S. Ren and Z. Xie, *Acc. Chem. Res.*, 2011, **44**, 299.
67 A. Sinha, T. Ghatak and J. K. Bera, *Dalton Trans.*, 2010, **39**, 11301.
68 M. Tanabe and K. Osakada, *Organometallics*, 2010, **29**, 4702.
69 E. Farnetti and S. Filipuzzi, *Inorg. Chim. Acta*, 2010, **363**, 467.
70 F. Blank and C. Janiak, *Coord. Chem. Rev.*, 2009, **253**, 827.
71 P. Mastrorilli, *Eur. J. Inorg. Chem.*, 2008, 4835.
72 G. Schmid, *Chem. Soc. Rev.*, 2008, **37**, 1909.
73 L. Pedrosa, *Synlett*, 2008, 1581.
74 G. Schmid, *Angew. Chem., Int. Ed.*, 2008, **47**, 3496.
75 A. B. Chaplin, *Chimia*, 2008, **62**, 217.
76 C. Lau, S. Ng, G. Jia and Z. Lin, *Coord. Chem. Rev.*, 2007, **251**, 2223.
77 S. Krompiec, N. Kuźnik, M. Krompiec, R. Penczek, J. Mrzigod and A. Tórz, *J. Mol. Catal. A: Chem.*, 2006, **253**, 132.
78 D. W. Allen and B. F. Taylor, *J. Chem. Soc., Dalton Trans.*, 1982, 51.
79 P. Arsenyan, A. Petrenko, K. Oberte and S. Belyakov, *Chem. Heterocycl. Compd.*, 2012, **48**, 1263.
80 F. N. Blanco, L. E. Hagopian, W. R. McNamara, J. A. Golen, A. L. Rheingold and C. Nataro, *Organometallics*, 2006, **25**, 4292.
81 M. Necas, M. Beran, J. D. Woollins and J. Novosad, *Polyhedron*, 2001, **20**, 741.
82 K. D. Reichl, C. L. Mandell, O. D. Henn, W. G. Dougherty, W. S. Kassel and C. Nataro, *J. Organomet. Chem.*, 2011, **696**, 3882.
83 S. Isenberg, S. Weller, D. Kargin, S. Valic, B. Schwederski, Z. Kelemen, C. Bruhn, K. Krekic, M. Maurer, C. M. Feil, M. Nieger, D. Gudat, L. Nyulaszi and R. Pietschnig, *ChemistryOpen*, 2019, **8**, 1235.
84 A. Lik, D. Kargin, S. Isenberg, Z. Kelemen, R. Pietschnig and H. Helten, *Chem. Commun.*, 2018, **54**, 2471.
85 A. Jakob, P. Ecorchard, M. Linseis, R. F. Winter and H. Lang, *J. Organomet. Chem.*, 2009, **694**, 655.
86 F. Barrière, R. U. Kirss and W. E. Geiger, *Organometallics*, 2005, **24**, 48.
87 P. Zanello, G. Opromolla, G. Giorgi, G. Sasso and A. Togni, *J. Organomet. Chem.*, 1996, **506**, 61.
88 C. L. Mandell, S. S. Kleinbach, W. G. Dougherty, W. S. Kassel and C. Nataro, *Inorg. Chem.*, 2010, **49**, 9718.
89 A. Orthaber, R. H. Herber and R. Pietschnig, *J. Organomet. Chem.*, 2012, **719**, 36.
90 M. Trivedi, S. K. Ujjain, G. Singh, A. Kumar, S. K. Dubey and N. P. Rath, *J. Organomet. Chem.*, 2014, **772–773**, 202–209.

91 D. Li, Y.-F. Luo, T. Wu and S. W. Ng, *Acta Crystallogr., Sect. E: Struct. Rep. Online*, 2004, **60**, m927.
92 M. Trivedi, R. Nagarajan, A. Kumar, N. P. Rath and P. Valerga, *Inorg. Chim. Acta*, 2011, **376**, 549.
93 S. P. Neo, Z.-Y. Zhou, T. C. W. Mak and T. S. A. Hor, *J. Chem. Soc., Dalton Trans.*, 1994, 3451.
94 P. Pinto, M. J. Calhorda, V. Félix, T. Avilés and M. G. B. Drew, *Monatsh. Chem.*, 2000, **131**, 1253.
95 C. Di Nicola, Effendy, C. Pettinari, B. W. Skelton, N. Somers and A. H. White, *Inorg. Chim. Acta*, 2005, **358**, 695.
96 J. Díez, M. P. Gamasa, J. Gimeno, M. Lanfranchi and A. Tiripicchio, *J. Organomet. Chem.*, 2001, **637–639**, 677.
97 M. Trivedi, G. Singh, A. Kumar and N. P. Rath, *Dalton Trans.*, 2014, **43**, 13620.
98 P. S. Prasad, M. K. Pandey and M. S. Balakrishna, *Polyhedron*, 2019, **158**, 173.
99 S. K. Gibbons, R. P. Hughes, D. S. Glueck, A. T. Royappa, A. L. Rheingold, R. B. Arthur, A. D. Nicholas and H. H. Patterson, *Inorg. Chem.*, 2017, **56**, 12809.
100 K. M. Gramigna, J. V. Oria, C. L. Mandell, M. A. Tiedemann, W. G. Dougherty, N. A. Piro, W. S. Kassel, B. C. Chan, P. L. Diaconescu and C. Nataro, *Organometallics*, 2013, **32**, 5966.
101 H. Tran-Vu and O. Daugulis, *ACS Catal.*, 2013, **3**, 2417.
102 L. Dang, Z. Lin and T. B. Marder, *Organometallics*, 2010, **29**, 917.
103 S. S. Zigler, L. M. Johnson and R. West, *J. Organomet. Chem.*, 1988, **341**, 187.
104 X. Wu, W. Zhang, X. Zhang, N. Ding and T. S. A. Hor, *Eur. J. Inorg. Chem.*, 2015, **2015**, 876.
105 J. Campos, M. F. Espada, J. Lopez-Serrano and E. Carmona, *Inorg. Chem.*, 2013, **52**, 6694.
106 G. R. Fulmer, A. J. M. Miller, N. H. Sherden, H. E. Gottlieb, A. Nudelman, B. M. Stoltz, J. E. Bercaw and K. I. Goldberg, *Organometallics*, 2010, **29**, 2176.
107 G. M. Sheldrick, *Acta Crystallogr., Sect. A: Found. Crystallogr.*, 2008, **64**, 112.
108 C. F. Macrae, P. R. Edgington, P. McCabe, E. Pidcock, G. P. Shields, R. Taylor, M. Towler and J. van de Streek, *J. Appl. Crystallogr.*, 2006, **39**, 453.
109 A. L. Spek, *Acta Crystallogr., Sect. C: Struct. Chem.*, 2015, **71**, 9.
110 C. F. Macrae, I. J. Bruno, J. A. Chisholm, P. R. Edgington, P. McCabe, E. Pidcock, L. Rodriguez-Monge, R. Taylor, J. van de Streek and P. A. Wood, *J. Appl. Crystallogr.*, 2008, **41**, 466.
111 I. Noviandri, K. N. Brown, D. S. Fleming, P. T. Gulyas, P. A. Lay, A. F. Masters and L. Phillips, *J. Phys. Chem. B*, 1999, **103**, 6713.